




Structural, optical and nuclear radiation shielding properties of strontium barium borate glasses doped with dysprosium and niobium

G. Sathiyapriya¹, K. A. Naseer¹, K. Marimuthu^{1,*}, E. Kavaz^{2,*} , A. Alalawi³, and M. S. Al-Buriahi⁴

¹Department of Physics, The Gandhigram Rural Institute Deemed University, Gandhigram 624 302, India

²Department of Physics, Ataturk University, 25240 Erzurum, Turkey

³Department of Physics, Umm AL-Qura University, Makkah, Saudi Arabia

⁴Department of Physics, Sakarya University, Sakarya, Turkey

Received: 10 December 2020

Accepted: 6 February 2021

Published online:

7 March 2021

© The Author(s), under exclusive licence to Springer Science+Business Media, LLC, part of Springer Nature 2021

ABSTRACT

Five new strontium barium borate (BNBD) glasses doped with dysprosium ion and different concentrations of niobium pentoxide were synthesized using the standard melt-quenching method. The physical, structural, optical and gamma radiation shielding properties of these glasses were investigated. Density, average molecular weight, refractive index, molar volume, optical dielectric constant, boron-boron separation, metallization criterion, oxygen packing density, Poisson ratio, optical basicity, optical electronegativity, and two-photon absorption coefficients of the synthesized glasses were determined. By the addition of Nb₂O₅ content, boron-boron distance and oxygen packing density values increased, while molar volume of oxygen decreased due to the formation of bridging oxygen. The two-photon absorption could be constrained by replacing BaCO₃ by niobium pentoxide content which further influences the bandgap. The ionic nature of the titled glasses is discussed using the bonding parameter, optical basicity, ionic and covalent characteristic parameter values. Moreover, the shielding ability of dysprosium ions doped niobium borate glasses against photons, fast neutrons and electrons has been extensively evaluated. For this purpose, the mass attenuation coefficient (μ/ρ , cm²/g) of the glasses and several photon protection parameters, derived from μ/ρ were obtained for 0.015–15 meV. The maximum μ/ρ values were achieved for BNBD0 glass, varying between 0.033 and 35.430 cm²/g. The lowest buildup factor values were found for BNBD0 glass. Furthermore, effective removal cross section values for fast neutrons increased steadily between 0.125 and 0.130 cm⁻¹ due to the increase in the density of the glasses with the enhancing of Nb₂O₅ concentration. It was noticed that the range of high energy electrons was shorter on the BNBD0 glass. It was concluded that BNBD0 glass with high BaCO₃

Address correspondence to E-mail: mari_ram2000@yahoo.com; esra.kavaz@atauni.edu.tr; esrakvz@gmail.com

concentration can be considered as an alternative material in nuclear radiation shielding applications.

1 Introduction

Glass is a transparent and non-crystalline solid material which exhibits the optical phenomenon like transmission, reflection, and refraction. Such material became main ingredient part in numerous applications in human daily life. The glassy material is widely used for making solid-state laser materials, making control rods in nuclear reactors due to its high thermal neutron absorption cross-section, data storage applications due to its high magnetic susceptibility, fabrication of photonic devices, and nuclear shielding applications such those are used in X-rays rooms [1–7].

B₂O₃ is present in nearly all commercially available glasses that are considered as one of the most common glass formers. These glasses have unique properties like low melting point, high thermal stability, and good solubility of rare earth ions. Such properties can be enhanced by the addition of modifiers such as alkali and alkaline earth ions [8–11]. The trivalent dysprosium ion (Dy³⁺) can combine with various non-metals at high temperatures to form binary compounds and it has superior downshifting luminescence properties [2, 3]. Dy³⁺ ions doped yttrium aluminium garnet (YAG:Dy) results the emission of photons of longer wavelength in the visible region. Such idea is the basis for novel generation of UV-pumped white light emitting diodes. Moreover, the addition of Nb₂O₅ plays a significant role to improve the glass structure due to the coordination state of Nb⁵⁺ and its interaction with other ions. Also, the incorporation of Nb₂O₅ has a positive influence on the physical, chemical and optical properties of glasses [12–16].

Finally, glasses for nuclear radiation shielding applications are, nowadays, an ongoing hot research topic of materials science. Different research groups are actively working on this topic to find better glasses for radiation shielding in nuclear medicine and at nuclear reactor sites, instead of concretes and PbO glasses due to their demerits as shielding materials [17–21]. It is known that the mixing of heavy metal oxides in the glass network led to improve the density of the prepared glasses [22–27].

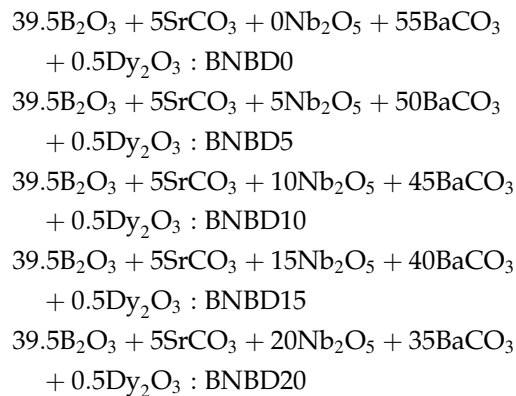
Kılıç et al. [28], investigated the physical, optical and shielding characteristics of Zinc-borate glasses depending on Er₂O₃ addition ratio and they reported that Er₂O₃ improved the material characteristics of the Zinc Borate glasses. Zakaly et al. [29] showed that Bi₂O₃ addition on lithium borate glasses increased the mechanical and radiation protecting capacity of the glasses. Zakaly et al. [29] also surveyed BaO effect on physical, structural, optical and shielding features of borosilicate glasses extensively. BaO enhanced the usability of the borosilicate glasses for optical and shielding applications. Glasses containing barium is an excellent preference for radioactive liquid waste disposal owing to its sulphate abiding capacity. It can lower the glass forming temperature of the borates, even without a cluster formation. It can be used as a barrier in plasma display ribs and as a γ -RS material. Strontium ions can improve the rigidity of the glass samples. Therefore, this may improve the ability of glass to attenuate the nuclear radiation to use for shielding applications for the further development of this topic by other researchers [30–32]. In literature, many glasses and their nuclear shielding features are principally reported by other research groups.

In the present work, five new strontium barium borate glasses doped with dysprosium ion and different concentrations of niobium pentoxide were synthesized using the standard melt-quenching method. The physical, optical, structural, and nuclear-shielding properties of the synthesized were investigated. For example, density (ρ), average molecular weight (M), refractive index (n_d), molar volume (V_m), optical dielectric constant, boron-boron separation (d_{B-B}), metallization criterion (M), oxygen packing density (OPD), Poisson ratio, optical basicity (A_{th}), optical electronegativity (χ_{opt}), and two-photon absorption coefficients (β) of the synthesized glasses were determined. To determine the radiation shielding capability of the fabricated glasses, the μ/ρ , HVL, ERCS, MFP, Z_{eff} , EBF and EABF were calculated [33–35]. Additionally, Total stopping power (TSP) and Continuous Slowing Down Approximation (CSDA) ranges of the glasses were obtained for electrons.

2 Experimental

2.1 Synthesis

Five new strontium barium borate glasses doped with dysprosium ion and different concentrations of niobium pentoxide were synthesized using the standard melt-quenching method [36] with the high purity (99.99%) analytical grade (from Sigma Aldrich) chemicals namely B_2O_3 , $SrCO_3$, Nb_2O_5 , $BaCO_3$ and Dy_2O_3 . Chemical composition (in wt %) and the glass codes are presented below.



In the present work, 15 g batch chemicals are weighed in a standard digital weighing balance. The batch mixtures are taken into an agate mortar and well grained to get fine homogeneous particles. This mixture is taken into the porcelain crucible and put inside a muffle furnace at 1250 °C for 2½ h. During melting, the crucible has been stirred periodically for the homogeneous mixing. The melted molten flux is poured onto a preheated rectangular brass plate in the desired groove (shape) and the glass is formed. The annealing is done at 420 °C for 10 h. The annealing process is made to ensure the improved mechanical strength, removal of air bubbles and defects due to quenching of the prepared glass samples. Finally, the prepared glass samples are then polished on both sides to obtain uniform thickness before it is taken for further structural/optical characterizing studies.

2.2 Characterization

The UV–Vis–NIR absorption spectra of the present glasses were recorded using JASCO 500 spectrophotometer in the wavelength region 200–1800 nm with a spectral resolution of ± 0.1 nm. The densities of the

prepared glass samples were determined using Archimedes principle, with xylene as a reference liquid. Using the Abbe refractometer, refractive indices of the prepared glasses were measured at a wavelength of 5893 Å with mono-bromonaphthalene as the contact liquid. All these measurements were carried out at room temperature (RT) only.

3 Results and discussion

3.1 Physical properties

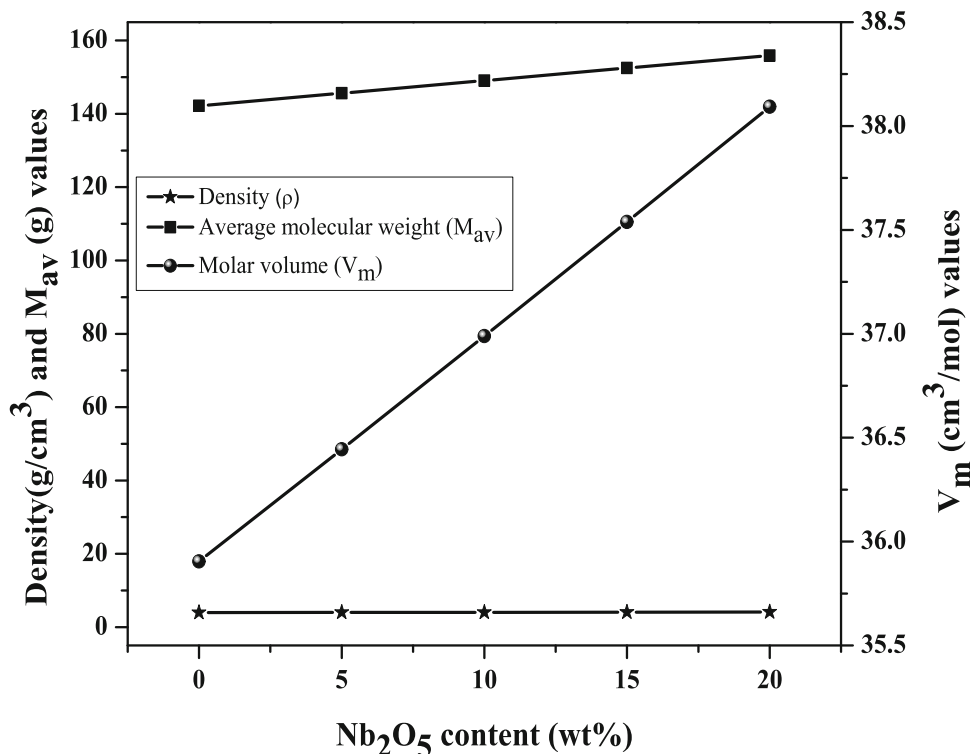
The physical properties of the prepared glasses were determined using the formulae reported in the literature [37, 38], and are listed in Table 1. The changes in density, average molecular weight and molar volume of the prepared glasses are presented in Fig. 1. Density and refractive index are used to study the network modifications due to the varying alkali content. The increasing trend in the density and molar volume indicates the formation of non-bridging oxygen's (NBOs) in the present glass network and the addition of rare earth ions increase the average molecular weight [39]. Molar volume is calculated by dividing the average molecular weight with density. Basically, density and molar volume are found to exhibit opposite trend, but in the present work both exhibit the similar trend due to the formation of non-bridging oxygen's. The density and molar volume values are found increase with increasing Nb_2O_5 content in the present glasses; hence the network is more open and less tightly packed [40].

Applying the theory of metallization of condensed matter proposed by Dimitrov [41], the nature of the solid either metallic or non-metallic is related to their density and refractive indices values. The theory on metallization condition is $R_m/V_m = 1$ in the Lorentz-Lorentz equation, and the necessary condition for metallic or non-metallic nature is, if $R_m/V_m < 1$ then it is non-metallic or if $R_m/V_m \geq 1$ then it is metallic. Hence the transition metal state is $M = 0$. Metallization criterion (M) is calculated using the equation, $M = 1 - (R_m/V_m)$, where R_m and V_m are the molar refractivity and molar volume of the present glass network. The calculated metallization criterion (M) values are presented in Table 1 [26].

Table 1 Physical properties of the Dy³⁺ ions doped Niobium Borate glasses

Physical properties	BNBD0	BNBD5	BNBD10	BNBD15	BNBD20
Density ρ (g/cm ³)	3.960	3.996	4.029	4.061	4.092
Refractive index n_d (589.3 nm)	1.643	1.667	1.684	1.702	1.721
Average molecular weight M (g)	142.208	145.631	149.055	152.478	155.902
Molar volume V_m (cm ³ /mol)	35.904	36.444	36.989	37.538	38.092
Optical dielectric constant ($P_{\frac{\partial \epsilon}{\partial P}}$)	1.699	1.778	1.835	1.896	1.961
Metallization criterion (M)	0.638	0.627	0.620	0.612	0.604

Fig. 1 Changes in density (ρ), molar volume (V_m) and average molecular weight (M_{av}) of Dy³⁺ ions doped Niobium Borate glasses as a function of increasing Nb₂O₅ content



3.2 Structural properties

3.2.1 Boron-Boron separation ($\langle d_{B-B} \rangle$), molar volume of oxygen (V_o), oxygen packing density (OPD)

The structural properties like boron–boron distance ($\langle d_{B-B} \rangle$), molar volume of oxygen (V_o) and oxygen packing density (OPD) are calculated using the related formulae reported in the literature [42–44]. Boric acid acts as a glass former in the present glass system; it has confirmed the compactness of glass network due to the addition of Nb₂O₅ content. The density and refractive index values are found to increase, and the molar volume of oxygen decreases with the increase in the formation of Nb₂O₅ in the present glass network, due to the replacement of lighter B₂O₃ (69.62 g/mol) by heavier Nb₂O₅ (265.81 g/mol).

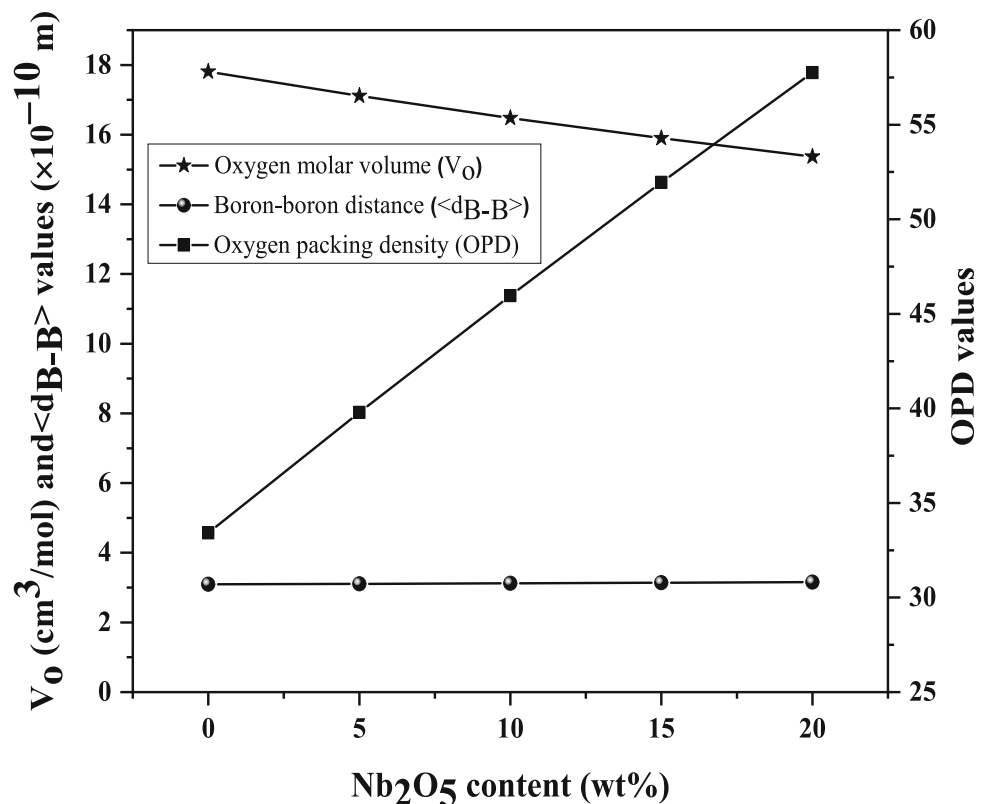
Boron-boron distance is found to increase with the addition of Nb₂O₅ content. The calculated values of ($\langle d_{B-B} \rangle$), V_o and OPD are presented in Table 2 and the relationship among these values are pictorially shown in Fig. 2. The oxygen packing density values are found to increase and the molar volume of oxygen decreases with the addition of Nb₂O₅ content which implies that the network is more tightly packed due to the formation of bridging oxygen (BO) [3, 16], it exhibits an opposite trend, and this behavior is represented as the fading of NBO and increment in BOs. In the present glass system Niobium acts as a modifier.

Table 2 The boron-boron separation ($d_{B-B} \times 10^{-10}$ m), molar volume of oxygen (V_o , cm^3/mol), oxygen packing density (OPD), average coordination number (n_{av}), number of bonds per unit volume

($n_b \times 1028 \text{ m}^{-3}$), Poisson ratio (μ_{cal}), optical electronegativity (χ_{opt}), optical basicity (A_{th}), two-photon absorption coefficient (β cm/GW) and R_m/V_m of the Dy^{3+} ions doped Niobium Borate glasses

Parameters	BNBD0	BNBD5	BNBD10	BNBD15	BNBD20
d_{B-B}	3.093	3.108	3.124	3.139	3.154
V_o	17.809	17.115	16.479	15.899	15.367
OPD	33.421	39.786	45.959	51.946	57.753
n_{av}	4.003	4.042	4.082	4.123	4.165
n_b	6.71	6.68	6.65	6.61	6.58
μ_{cal}	0.282	0.280	0.279	0.276	0.275
χ_{opt}	1.895	1.850	1.819	1.786	1.753
A_{th} (n_d)	0.431	0.459	0.486	0.510	0.532
β	13.647	12.432	11.986	11.662	10.447
R_m/V_m	0.361	0.372	0.379	0.387	0.395

Fig. 2 The variation of oxygen molar volume (V_o), oxygen packing density (OPD) and boron-boron separation ($\langle d_{B-B} \rangle$) of Dy^{3+} ions doped Niobium Borate glasses as a function of increasing Nb_2O_5 content



3.2.2 Nearest neighbor coordination (n_{av}), bonds per unit volume (n_b) and Poisson's ratio (μ_{cal})

Average coordination number is one of the most important parameters to calculate the formation of bridging (BO) or non-bridging oxygen (NBO). The average coordination number n_{av} is calculated using the formula, [38] $n_{av} = \sum_i (x n_c)_i$ where n_c is the cation coordination number. The values of n_{av} is reported in

Table 2, and for the present glass network, average coordination number value is found to increase which indicates the increase in the number of bridging oxygen's. Generally, the average coordination number or nearest neighbor coordination number value is found to increase with the increase in Nb_2O_5 content due to the formation of number of bridging oxygen's. The coordination number of boron, strontium, niobium, barium and dysprosium

Fig. 3 Composition dependence of optical electronegativity (χ_{opt}), basicity (A_{th}), covalent factor (C_c) and ionic factor (I_c) with respect to increasing Nb_2O_5 content in the Dy^{3+} ions doped Niobium Borate glasses

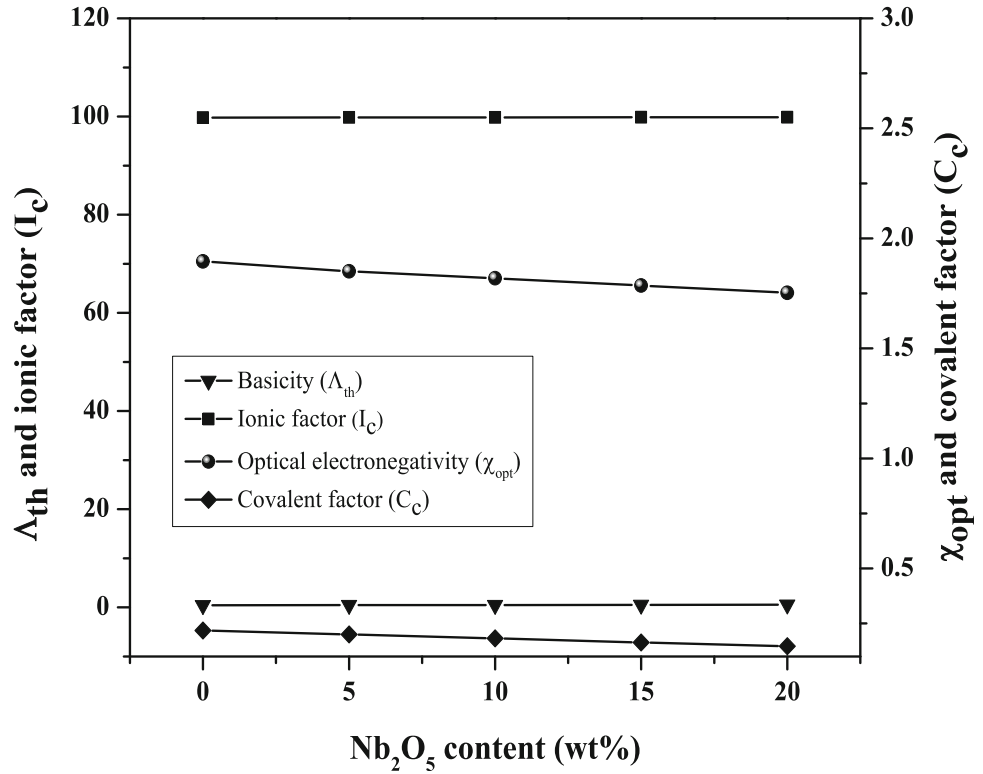


Table 3 Electro negativity (ΔX), ionic character factor (I_c , %) and covalent character factor (C_c , %) of the Dy^{3+} ions doped Niobium Borate glasses

Glass chemical	Electro negativity of elements	X_C	X_A	ΔX	I_c (%)	C_c (%)
B_2O_3	B (2.04), O (3.44)	4.08	10.32	6.24	99.99	0.01
$SrCO_3$	Sr (0.95), CO_3 (5.64)	0.95	5.64	4.69	99.59	0.41
Nb_2O_5	Nb (1.6), O (3.44)	3.2	17.2	14	100	0
$BaCO_3$	Ba (0.89), CO_3 (5.64)	0.89	5.64	4.75	99.64	0.36
Dy_2O_3	Dy (1.22), O (3.44)	2.44	10.32	7.88	99.99	0.01
$39.5B_2O_3 + 5SrCO_3 + 0Nb_2O_5 + 55BaCO_3 + 0.5Dy_2O_3$					99.781	0.218
$39.5B_2O_3 + 5SrCO_3 + 5Nb_2O_5 + 50BaCO_3 + 0.5Dy_2O_3$					99.799	0.200
$39.5B_2O_3 + 5SrCO_3 + 10Nb_2O_5 + 45BaCO_3 + 0.5Dy_2O_3$					99.817	0.182
$39.5B_2O_3 + 5SrCO_3 + 15Nb_2O_5 + 40BaCO_3 + 0.5Dy_2O_3$					99.835	0.164
$39.5B_2O_3 + 5SrCO_3 + 20Nb_2O_5 + 35BaCO_3 + 0.5Dy_2O_3$					99.852	0.147

are found to be 4, 4, 6, 4 and 6, respectively. The bond density is affected by the addition of niobium oxide and is calculated using the below given formula [37],

$$n_b = \frac{N_A}{V_m} \sum_i (x n_c)_i = \frac{N_A}{V_m} n_{av} \tag{1}$$

where n_c is the coordination number of cations, N_A is the Avogadro number and x is the mole fraction of the particular oxides. The calculated number of bond values is reported in Table 2 and the values are found to decrease from 6.71 to 6.58 while increasing the Nb_2O_5 content. The number of bond (n_b) values decreases due to the formation of more number of

bridging oxygen's, where Nb_2O_5 act as the network modifier [45]. Poisson's ratio (μ_{cal}) values for a particular glass can be calculated theoretically using the following equations [45, 46],

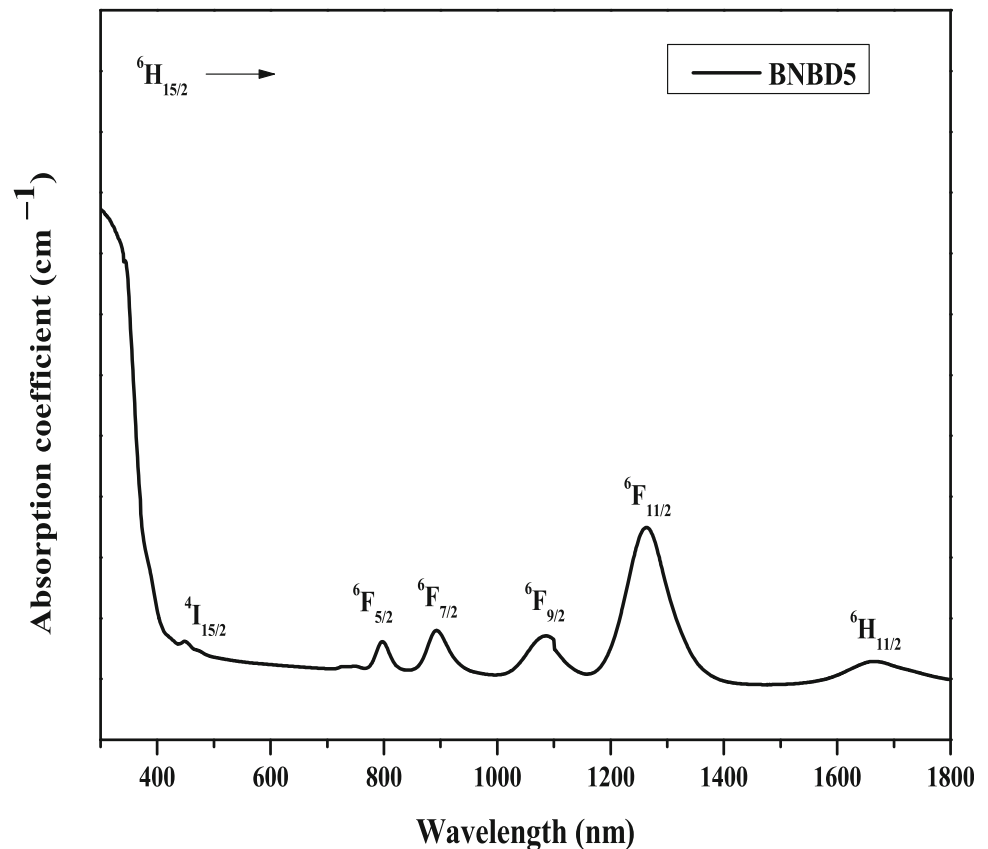
$$\mu_{cal} = 0.5 - \frac{1}{7.2V_t}, \text{ where.}$$

$$V_t = \frac{\rho_{glass}}{M_{glass}} \sum_i x_i v_i, \text{ and}$$

$$V_i = \frac{4\pi N_A}{3} (nr_A^3 + mr_O^3) \tag{2}$$

where V_t is the packing density, V_i is the oxide(s) packing factor $A_n O_{mv}$, M_{glass} is the molecular

Fig. 4 Absorption spectrum of the Dy³⁺ ions doped Niobium Borate glass



weight of the glass sample, r_O and r_A are the ionic radii of anion O and cation A, respectively [46]. The calculated Poisson's ratio values are shown in Table 2, and the observed Poisson's ratio values are found to decrease from 0.282 to 0.275. The calculated μ_{cal} values decrease thus increase the cross-link density. Generally, the cross-link density μ_{cal} which lie in the order 0.1–0.2 is the high cross-link density and 0.3–0.5 is the low cross-link density. In the present glass network Poisson's ratio value is found to be 0.2, thus the system possesses high-cross link density.

3.2.3 Photonic view of glasses (TPA)

Two-photon absorption coefficient (TPA) parameter has an important role in solid state physics; it is a non-linear optical process in which a molecule absorbs two photons at the same time. The two-photon absorption coefficient (β) is calculated using the formula, [4]

$$\beta(\text{cm/GW}) = [36.76 - 8.1E_g] \quad (3)$$

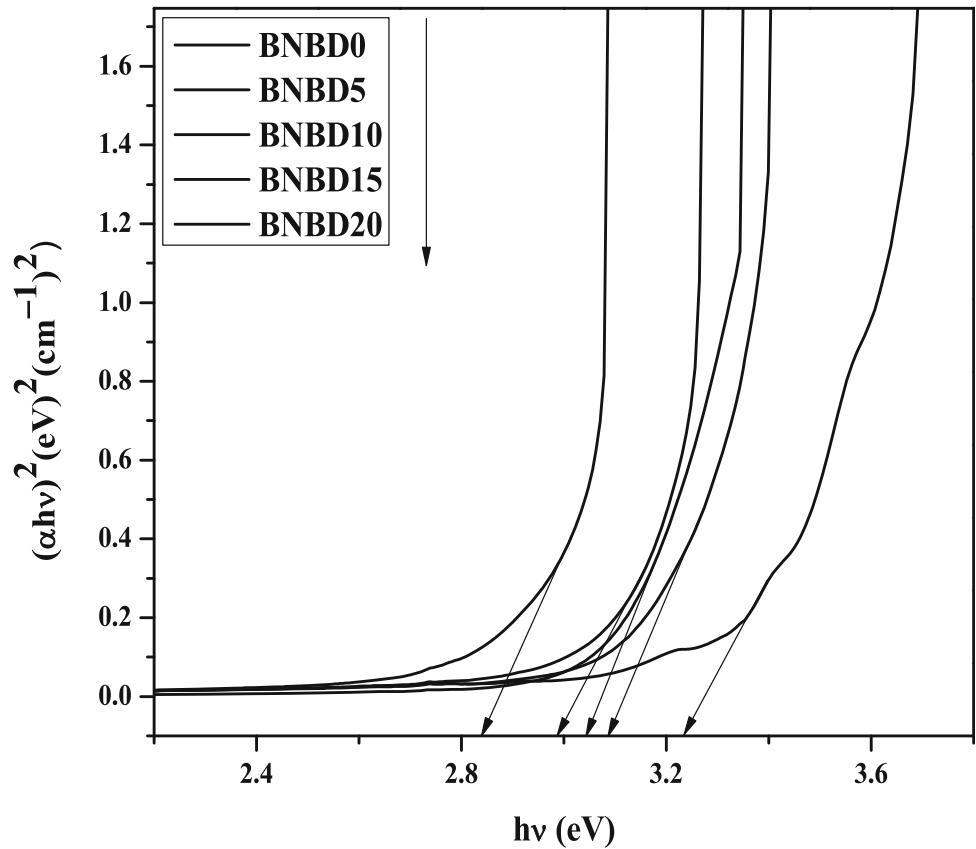
where E_g is the optical bandgap. TPA can put crucial restrictions on the optical waveguide; all optical switching devices and it possess one of the most fundamental radiation-matter connection systems. The two-photon absorption coefficient (β) values are found to decrease from 13.64 to 10.44 cm/GW and the obtained TPA values of the present glasses are shown in Table 2. TPA qualities could be constrained by replacing B_2O_3 with Nb_2O_5 which further influences the bandgap values. The β values pertaining to the E_{opt} in the present glass framework shows that the TPA relies on the electronic structure of the materials [37].

3.2.4 Basicity (Λ_{th}), optical electronegativity (χ_{opt}), covalency and ionicity

The theoretical optical basicity can be determined using the following equation [32]:

$$\Lambda_{th} = \sum_i^n x_i \Lambda_i \quad (4)$$

Fig. 5 Tauc’s plot for the direct allowed transitions in the Dy³⁺ ions doped Niobium Borate glasses



where $x_1, x_2, x_3, \dots, x_n$ are the equivalent fractions of different oxides (mole %) and $\Lambda_1, \Lambda_2, \Lambda_3, \dots, \Lambda_n$ are the optical basicity of the constituent oxides [10]. Polarizability is related to optical basicity values; the basicity values are presented in Table 2 and it is observed that the value increases from 0.431 to 0.532 due to the increase in Niobium oxide content. Optical electro negativity is calculated using the formula [22], $\chi_{opt} = 9.8e^{-n_d}$ where n_d is the refractive index. The optical electronegativity is one of the finest parameters which shows the nature of chemical bonding [47]. The relationship of basicity Λ_{th} , optical electronegativity (χ_{opt}), covalent factor (C_c) and ionic factor (I_c) with respect to niobium oxide (Nb_2O_5) values (0 to 20 wt%) are shown in Fig. 3 and the χ_{opt} values are reported in Table 3. The reported refractive index n values are based upon the optical electronegativity of χ_{opt} for different simple oxide materials and n are the basic fundamental property of the particular material; it is profoundly identified to the electronic polarizability.

Pauli’s electronegativity is used to calculate the ionic/covalent bonding nature of the present glasses using the formula [38],

$$C_{ionic}(I_c, \%) = [1 - \exp\{-0.25(\Delta\chi^2)\}] \times 100$$

$$C_{covalent}(C_c, \%) = \exp\{-0.25(\Delta\chi^2)\} \times 100 \tag{5}$$

where C_{ionic} is the ionic factor of I_c and $C_{covalent}$ denote the covalent factor of C_c , and $\Delta\chi$ represents the Pauli electronegativity. Optical absorption for semiconductor (insulator) through the electron change from valence band to conduction band and the transfer of electron from anion to cation is represented as the “electron transfer” (charge transfer absorption) is associated with the optical absorption. The Dysprosium ions doped Niobium Borate glasses are highly ionic in nature and the values are reported in Table 3. In the present glasses, covalent factor is 1% and the ionic factor is 99%, and the prepared glass sample in the present system is exceptionally ionic in nature than covalent nature [37].

Fig. 6 Tauc's plot for the indirect allowed transitions in the Dy³⁺ ions doped Niobium Borate glasses

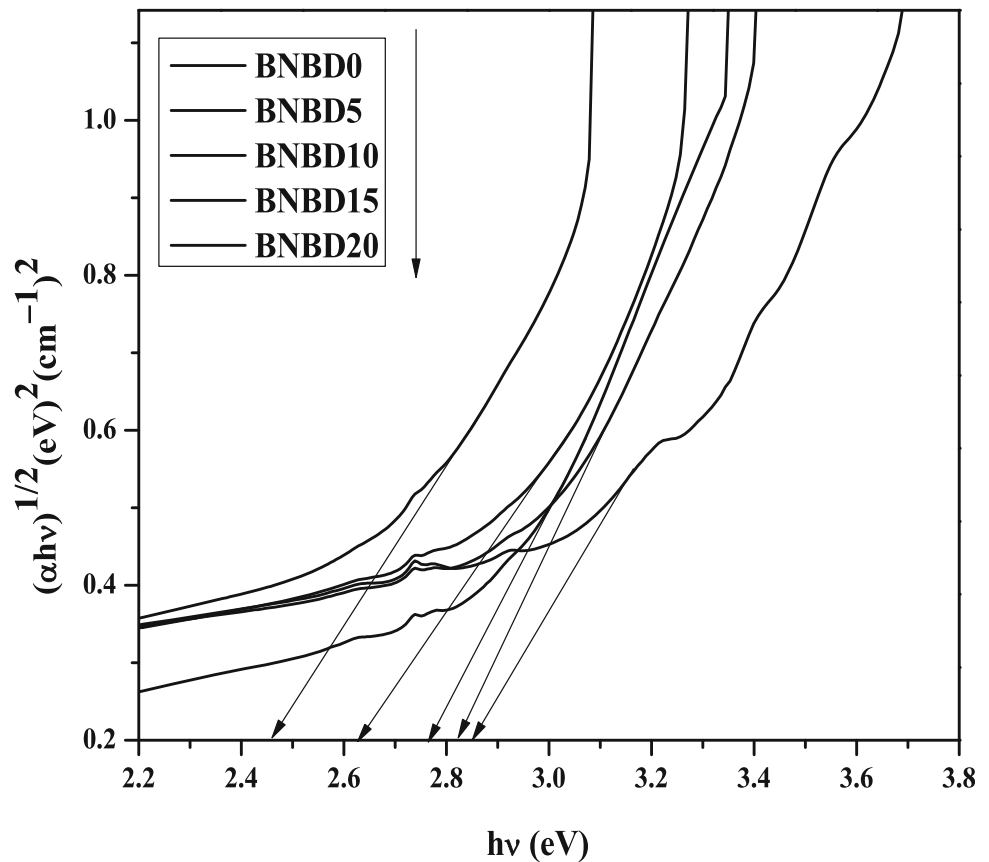


Table 4 The fundamental absorption edge (λ_{edge}), optical bandgap (E_{opt}), band tailing parameter (B) corresponding to the direct ($n = 1/2$) and indirect ($n = 2$) allowed transitions and Urbach's energy (ΔE) of the Dy³⁺ ions doped Niobium Borate glasses

Glass code	λ_{edge}	$n = 1/2$		$n = 2$		ΔE (eV)
		E_{opt} (eV)	B (cm ⁻¹ eV) ²	E_{opt} (eV)	B (cm ⁻² eV) ^{1/2}	
BNBD0	380	3.2361	20.8956	2.8523	2.5630	0.8072
BNBD5	383	3.0864	16.2781	2.8247	1.9271	1.1105
BNBD10	387	3.0462	14.9547	2.7636	1.6435	1.3670
BNBD15	389	2.9973	10.8012	2.6299	1.5766	1.7637
BNBD20	395	2.8439	7.9095	2.4595	1.3767	2.1042

3.3 Optical properties

3.3.1 Absorption spectra

Optical absorption spectra of the prepared glasses have been recorded in the wavelength region 300–1800 nm and as a representative case absorption spectrum of the Dy³⁺ ions doped BNBD5 glass is shown in Fig. 4. The spectrum exhibit f – f transitions centered at 450, 799, 892, 1093, 1264 and 1669 nm corresponds to the absorption transitions originates from ⁶H_{15/2} ground state to the other

excited states ⁴I_{15/2}, ⁶F_{5/2}, ⁶F_{7/2}, ⁶F_{9/2}, ⁶F_{11/2} and ⁶H_{11/2} [48–50]. The ⁶F_{11/2} hypersensitive transition is higher intense compared to the other observed transitions; hypersensitive transitions are the transitions which obey the selection rules, $\Delta S = 0$, $\Delta L \leq 2$ and $\Delta J \leq 2$ [51, 52].

3.3.2 Optical bandgap (E_{opt}) and Urbach's energy (ΔE) analysis

Mott and Davis theory derived from the absorption coefficient $(\alpha hv) = B (hv - E_g)^n$, where h is the

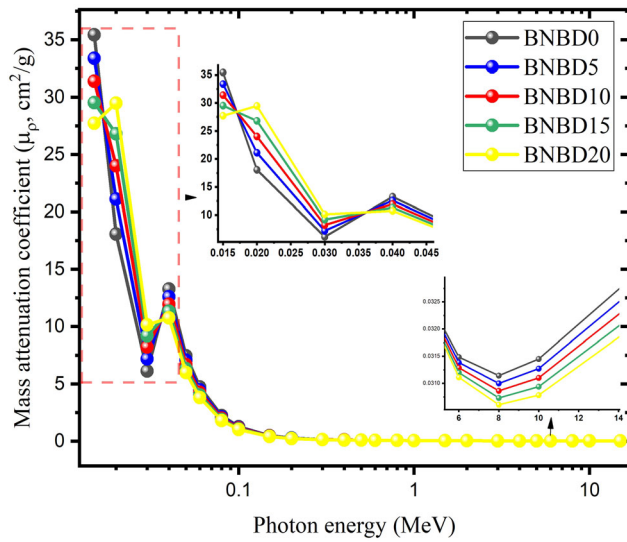


Fig. 7 The change of mass attenuation coefficient (μ/ρ) values as a function of photon energy for BNBD glasses

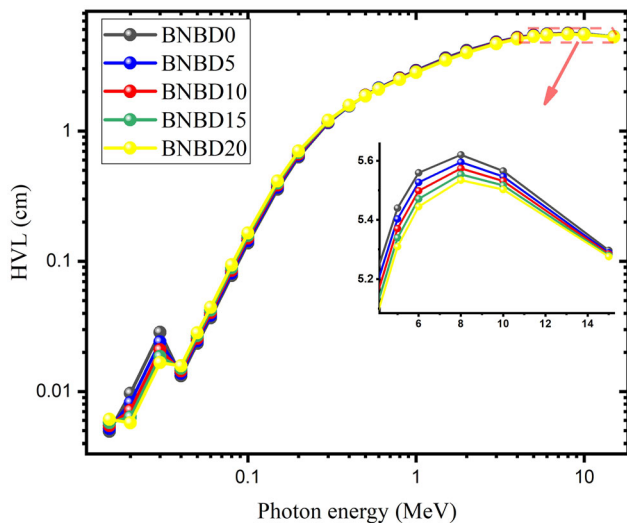


Fig. 8 HVL values of BNBD glasses versus the photon energy

incident radiation photon energy, n is an index which can have values as 2 and $1/2$, E_g is the optical bandgap and B is the band tailing parameter [53]. The optical bandgap is one of the significant parameters to analyze the solid-state materials for different photonic applications. Bandgap E_g values are calculated (i) $(\alpha hv)^2 = 0$ for the direct transition and (ii) $(\alpha hv)^{1/2} = 0$ for the indirect transition, using the Tauc's plot. Dysprosium ions doped Niobium Borate glasses Tauc's plot for the direct transition is shown in Fig. 5 and the indirect allowed transition Tauc's plot are shown in Fig. 6, and the direct, indirect bandgap values are reported in Table 4. The direct bandgap

values decrease from 3.23 to 2.84 while the indirect bandgap values decreases from 2.8523 to 2.4595 with the increase in Niobium content [54, 55]. By investigating the variation in the bandgap values of the Niobium containing glasses, it is evident that the created NBO bound an energized electron less firmly than the bonded oxygen and the NBO turns out to be more polarizable than the connecting oxygen which is commended by the higher basicity values. The disorderliness in the prepared glasses is measured by Urbach's energy (ΔE) values using the formula $\frac{\ln \alpha(v)}{(hv)} = \frac{1}{\Delta E}$, the width of the forbidden state present in the energy gap of an indistinct or disarranged material can be estimated through the proportional slope of photon energy versus logarithm of the absorption coefficient. The calculated Urbach's energy values are reported in Table 4, and the values are found to vary from 0.807 to 2.104. The Urbach's energy identified with the optical change between the last parts of the valence band which is reached out into the bandgap. The variation in the ΔE values is due to the deformities delivered inside the limited states [11]. The bandgap and the Urbach's energy values pursue the dissimilar pattern, when the bandgap values diminish the Urbach's energy values are found to increase because of the niobium ions content in the prepared glasses which may delocalize a portion of the forbidden states present in the energy levels through the supplementary adjustment in the glass structure. The absorption edge λ_{edge} , band tailing parameter B , and Urbach's energy ΔE values of the Dysprosium ions doped Niobium Borate glasses are reported in Table 4.

3.4 Nuclear shielding capability of the glasses

In this part of the study, it is aimed to determine the shielding effectiveness of the prepared glasses containing several ratios of Nb_2O_5 against different types of radiation. Firstly, the μ/ρ for the gamma-ray shielding features of the studied glasses, encoded BNBD0, BNBD5, BNBD10, BNBD15 and BNBD20, were obtained in the 0.015–15 meV photon energy range. Given the mixture of elements, as in the BNBD glasses fabricated in this study, the μ/ρ values are theoretically calculated by the following relation with the XCOM program [56];

Fig. 9 Comparison of MFPs for BNBD glasses with previously reported shielding materials

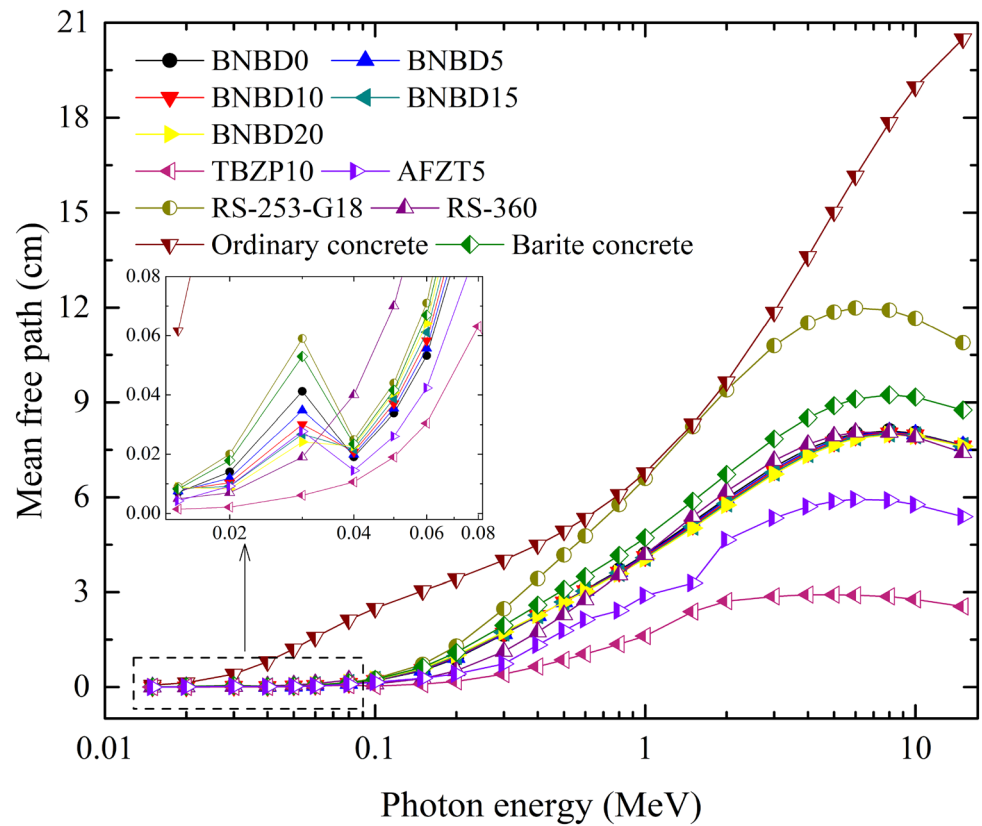


Fig. 10 Variations of effective atomic numbers of the BNBD glasses versus the photon energy

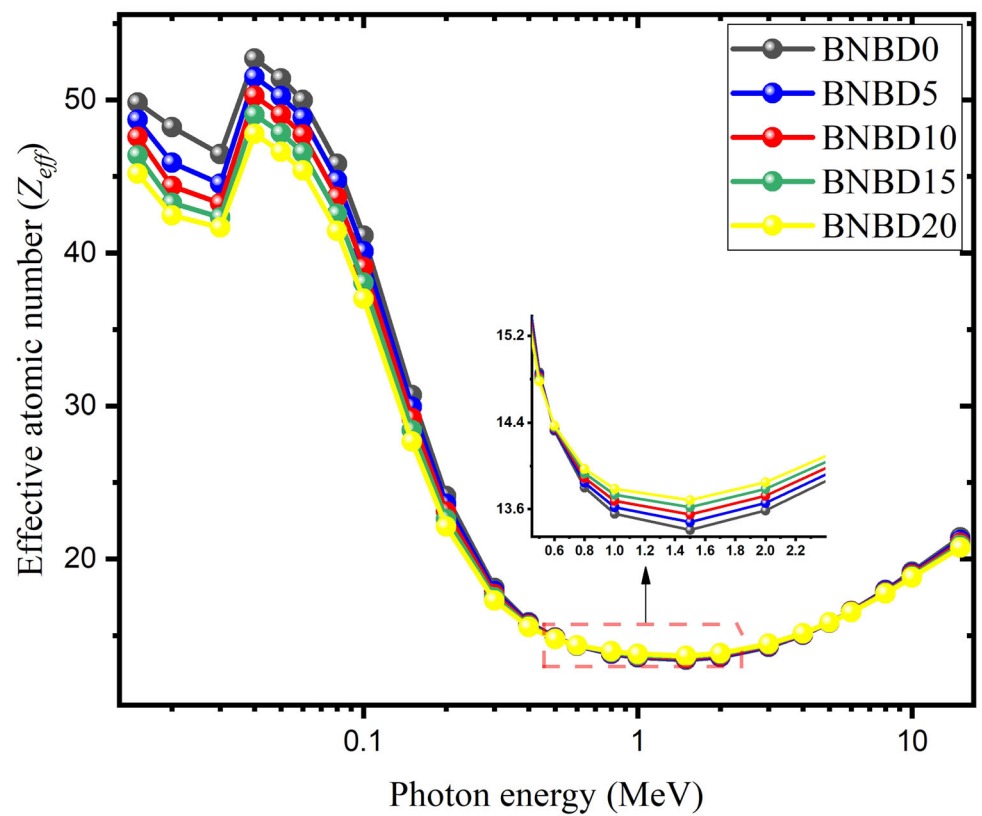
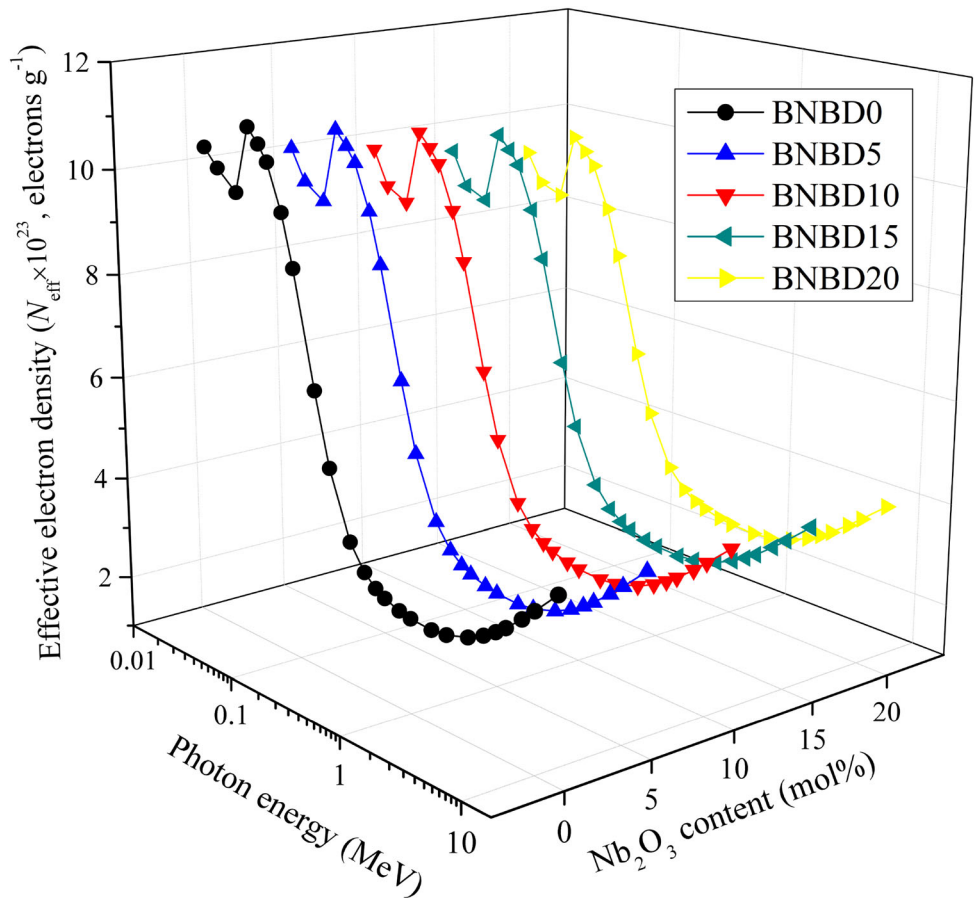


Fig. 11 Variations of effective electron density of the BNBD glasses versus the photon energy



$$\mu_{\rho} = \sum_i w_i(\mu/\rho)_i \tag{6}$$

Figure 7 depicts the change of the μ/ρ values of the BNBD glasses versus the energy of gamma photons. The largest μ/ρ values were gotten for low energy interval for all BNBD glasses. As the photon energy grows from 0.015 to 0.1 meV, the μ/ρ of the glasses drop swiftly due to photoelectric absorption (PEA) interaction whose cross section varies with $Z^{4-5}/E^{3.5}$. However, it is noticed that there are surprise increments in μ/ρ values around 0.02 meV and 0.04 meV for all BNBD glasses. These risings correspond to the K-shell absorption edges of Nb and Ba elements (18.98 ve 37.44 keV, respectively) in the chemical composition of the glasses. These abrupt peaks indicate that the probability of the interaction of photons with the glass increases at the absorption edges. The photons are roughly fully absorbed in PEA process. The decrements in μ/ρ values of the BNBD glasses are fairly slow in the range of 0.1–2 meV. Compton scattering (CS) mechanism, which varies according to Z/E , is responsible for this change. Therefore, in

medium energies, all BNBD glasses own almost the same μ/ρ values. After 2 meV, the gamma photons are under the impact of pair production (PP). Since the cross section of PP is proportional to the square of the atomic number of the scattering material, the μ/ρ values rise again between 2 and 15 meV. The BNBD0 glass with the highest BaCO₃ content gets the highest μ/ρ values, ranging from 0.033 to 35.430 cm²/g, while the smallest μ/ρ values, varying between 0.0321 and 27.722 cm²/g were obtained for the BNBD20 glass.

HVL (Half Value Layer) is a beneficial quantity to investigate gamma-ray protecting potential of a material. HVL is the thickness that diminishes the incident beam intensity by half and is determined by enforcing the ensuing equation [56];

$$HVL = (\ln 2/\mu). \tag{7}$$

The changing of HVL values with photon energy for BNBD glasses is shown in Fig. 8. According to Fig. 8, the chemical composition and density of the BNBD glasses have an influence upon HVL values.

Table 5 Equivalent atomic numbers and G-P Fitting Parameters of EABF and EBF for BNBD0 sample

Energy (MeV)	Z_{eq}	GP- fitting parameters									
		EBF					EABF				
		b	a	c	Xk	d	b	a	c	Xk	d
0.015	19.36	1.01	0.301	0.4	9.79	- 0.3426	1.009	0.357	0.28	11.79	- 0.2347
0.02	20.7	1.015	0.4	0.237	10.96	- 0.1539	1.016	0.355	0.256	12.17	- 0.1925
0.03	21.37	1.05	0.373	0.217	16.0	- 0.1682	1.049	0.352	0.241	14.33	- 0.1573
0.04	36.88	2.856	0.34	0.116	24.73	- 0.0935	1.329	0.364	0.111	28.16	- 0.1451
0.05	37.66	2.418	0.131	- 0.088	15.46	- 0.0074	1.289	0.141	0.008	10.81	0.0335
0.06	38.33	1.046	0.509	0.151	14.08	- 0.0714	1.051	0.464	0.175	13.81	- 0.0902
0.08	39.0	1.09	0.362	0.258	13.33	- 0.1685	1.117	0.271	0.347	13.39	- 0.2418
0.1	39.43	1.139	0.396	0.236	13.15	- 0.1516	1.194	0.301	0.324	14.12	- 0.2263
0.15	39.97	1.278	0.491	0.18	13.12	- 0.1049	1.515	0.315	0.314	12.94	- 0.2176
0.2	40.26	1.375	0.611	0.126	14.51	- 0.0692	1.811	0.421	0.233	14.16	- 0.1406
0.3	40.77	1.56	0.756	0.078	14.29	- 0.0521	2.345	0.559	0.171	14.02	- 0.1213
0.4	41.06	1.67	0.873	0.043	13.97	- 0.0355	2.57	0.699	0.112	13.88	- 0.0883
0.5	41.42	1.723	0.949	0.023	14.13	- 0.0269	2.595	0.789	0.081	13.84	- 0.0729
0.6	41.61	1.751	1.003	0.011	14.0	- 0.0233	2.547	0.856	0.061	13.74	- 0.0642
0.8	41.68	1.759	1.036	- 0.001	13.71	- 0.0142	2.405	0.914	0.038	13.52	- 0.046
1	41.52	1.745	1.065	- 0.007	13.49	- 0.0129	2.259	0.966	0.024	13.42	- 0.038
1.5	38.35	1.67	1.134	- 0.026	13.9	0.0022	1.917	1.096	- 0.015	11.79	- 0.0093
2	32.9	1.672	1.113	- 0.018	10.1	- 0.0071	1.844	1.085	- 0.012	10.76	- 0.013
3	27.92	1.62	1.059	- 0.004	12.13	- 0.0141	1.677	1.039	0.001	12.33	- 0.0177
4	26.17	1.553	1.026	0.005	12.93	- 0.0195	1.564	0.997	0.014	13.96	- 0.0295
5	25.44	1.485	1.007	0.012	13.13	- 0.0256	1.478	0.969	0.024	14.18	- 0.0378
6	24.93	1.445	0.977	0.023	13.34	- 0.0347	1.4	0.972	0.024	14.11	- 0.0377
8	24.48	1.359	0.967	0.029	13.62	- 0.041	1.306	0.952	0.033	13.63	- 0.0427
10	24.2	1.301	0.945	0.041	13.87	- 0.0523	1.246	0.943	0.04	14.17	- 0.0491
15	24.16	1.205	0.946	0.049	14.24	- 0.0582	1.153	0.956	0.043	14.59	- 0.049

Three separate photon-matter interactions are efficient in the variation of HVL values against photon energy. It is noteworthy that while the BNBD20 glass has the lowest HVL values among the other BNBD glasses in the low and high energy regions, the lowest HVL values are obtained for the BNBD0 glass at medium energies. In this result, it is effective that the cross-sections of PEA and PP vary depending on Z^{4-5} and Z^2 , respectively.

MFP (Mean Free Path) estimates the traveled interval among two running collisions by the gamma photons and can be achieved by the next relation [1];

$$Z_{\text{eff}} = \frac{\sum_i f_i A_i \left(\frac{\mu}{\rho}\right)_i}{\sum_j \frac{A_j}{Z_j} \left(\frac{\mu}{\rho}\right)_j} \quad (8)$$

Figure 9 presents the comparison of MFP values of the BNBD glasses with some previously reported shielding materials, TBZP10 glass [7], AFZT5 glass [57], RS-253-G18, RS-36 commercial glasses [58] and ordinary and barite concretes [59]. Small MFP values mean the shield material is better at attenuating gamma photons. In Fig. 9, the manufactured glasses possess smaller MFP values than ordinary and barite-added concretes and RS-253-G18 glass, while the MFPs of BNBD glasses are thicker than those of RS-360 and AFZT5 glasses. Maximum of 8 cm MFP was achieved for BNBD glasses even at the highest energies. It is noticed from Fig. 9 that since the density of the BNBD glasses is very close to each other, the MFP values are almost the same.

The effective atomic number (Z_{eff}) is needed to represent materials included multiple elements with

Table 6 Equivalent atomic numbers and G-P Fitting Parameters of EABF and EBF for BNBD5 sample

Energy (MeV)	Zeq	GP- fitting parameters									
		EBF					EABF				
		b	a	c	Xk	d	b	a	c	Xk	d
0.015	19.01	1.012	0.133	0.616	11.36	- 0.6118	1.01	0.226	0.42	12.97	- 0.4321
0.02	21.56	1.015	0.352	0.306	11.03	- 0.2367	1.015	0.338	0.268	13.25	- 0.2109
0.03	22.27	1.045	0.373	0.211	18.82	- 0.1997	1.044	0.345	0.243	15.29	- 0.1645
0.04	36.31	2.74	0.339	0.124	24.07	- 0.0937	1.31	0.366	0.116	27.99	- 0.1544
0.05	37.07	2.337	0.144	- 0.068	15.3	- 0.0154	1.276	0.154	0.022	10.93	0.0231
0.06	37.75	1.049	0.501	0.156	14.05	- 0.0749	1.055	0.457	0.179	13.85	- 0.0935
0.08	38.41	1.095	0.366	0.255	13.36	- 0.1655	1.124	0.277	0.34	13.44	- 0.2355
0.1	38.78	1.147	0.402	0.232	13.19	- 0.1484	1.205	0.314	0.313	14.41	- 0.2188
0.15	39.3	1.291	0.5	0.175	13.16	- 0.1023	1.547	0.324	0.308	12.97	- 0.2133
0.2	39.52	1.393	0.624	0.122	14.46	- 0.0673	1.856	0.435	0.227	14.12	- 0.1378
0.3	39.94	1.578	0.772	0.073	14.19	- 0.0501	2.38	0.58	0.163	13.95	- 0.117
0.4	40.24	1.683	0.888	0.039	13.82	- 0.0342	2.583	0.721	0.105	13.78	- 0.0851
0.5	40.38	1.737	0.966	0.019	13.83	- 0.0257	2.596	0.815	0.074	13.68	- 0.069
0.6	40.65	1.759	1.016	0.008	13.65	- 0.0224	2.543	0.877	0.055	13.55	- 0.061
0.8	40.52	1.766	1.051	- 0.004	13.19	- 0.0141	2.395	0.937	0.033	13.15	- 0.0434
1	40.97	1.748	1.071	- 0.008	13.26	- 0.0128	2.254	0.975	0.022	13.19	- 0.0369
1.5	37.65	1.674	1.137	- 0.027	14.19	0.0028	1.92	1.1	- 0.016	11.56	- 0.0092
2	31.97	1.677	1.115	- 0.019	9.83	- 0.0065	1.842	1.092	- 0.013	10.47	- 0.0112
3	27.42	1.622	1.059	- 0.005	12.1	- 0.0139	1.679	1.038	0.002	12.36	- 0.0179
4	25.84	1.554	1.026	0.005	12.91	- 0.019	1.566	0.996	0.014	13.91	- 0.0295
5	25.05	1.487	1.005	0.012	13.13	- 0.0254	1.479	0.968	0.024	14.2	- 0.0374
6	24.58	1.446	0.976	0.023	13.33	- 0.0344	1.401	0.97	0.024	14.04	- 0.0376
8	24.08	1.36	0.965	0.03	13.61	- 0.0406	1.308	0.95	0.034	13.53	- 0.0422
10	23.9	1.302	0.944	0.04	13.85	- 0.0517	1.248	0.94	0.04	14.15	- 0.0493
15	23.73	1.206	0.943	0.049	14.21	- 0.0579	1.155	0.956	0.042	14.57	- 0.0479

a single atomic number, and in this study, it was calculated by the direct method given below [60];

$$N_{el} = N_A Z_{eff} \frac{1}{\langle A \rangle} \tag{9}$$

where f_i is the fractional abundance of i th element according to the number of atoms and A_i represent the atomic weight of the i th element in the material. Also, Z_j represents the atomic number. Figure 10 displays the varying Z_{eff} values of BNBD glasses with different Nb_2O_5 and $BaCO_3$ concentrations depending on the photon energy. As exposed in Fig. 10, Z_{eff} gains the highest values in the low energy region due to PEA process and an abrupt fall is seen in Z_{eff} values towards 0.1 meV photon energy. The Z_{eff} values of the BNBD glasses rise with decreasing Nb_2O_5 contribution in the investigated glasses. In medium energies, the Z_{eff} s of all glasses are the

smallest. Beyond 1.022 meV, where Pair Production prevails, Z_{eff} values again enhance. It is clear that the BNBD0 glass with the largest $BaCO_3$ content generally takes the largest Z_{eff} s ranging from 49.83–13.40 in all photon energies. In addition, using Z_{eff} values, the effective electron density (N_{el}) of the BNBD glasses was calculated from Eq. 9 [61];

$$N_{el} = N_A Z_{eff} \frac{1}{\langle A \rangle} \tag{10}$$

Here, $\langle A \rangle$ denotes the mean atomic mass of the glass and N_A refers to Avogadro number. Figure 11 represents that the N_{el} curves can be interpreted in a similar approach to Z_{eff} . However, unlike Z_{eff} , the N_{el} values are affected by the $\langle A \rangle$'s of the glasses. Figure 11 indicates that the BNBD0 glass with the largest $\langle A \rangle$ owns the lowest N_{el} values, since N_{el} is inversely proportional to $\langle A \rangle$.

Table 7 Equivalent atomic numbers and G-P Fitting Parameters of EABF and EBF for BNBD10 sample

Energy (MeV)	Z _{eq}	GP- fitting parameters									
		EBF					EABF				
		b	a	c	Xk	d	b	a	c	Xk	d
0.015	18.67	1.011	0.249	0.464	17.26	− 0.5082	1.01	0.312	0.33	18.34	− 0.3864
0.02	22.32	1.014	0.311	0.364	11.1	− 0.3072	1.014	0.323	0.277	14.17	− 0.2265
0.03	23.09	1.041	0.373	0.206	21.28	− 0.2271	1.04	0.338	0.245	16.13	− 0.1708
0.04	35.69	2.61	0.338	0.133	23.34	− 0.0939	1.289	0.368	0.122	27.79	− 0.1646
0.05	36.47	2.253	0.158	− 0.047	15.14	− 0.0237	1.262	0.167	0.037	11.06	0.0122
0.06	37.15	1.053	0.492	0.161	14.02	− 0.0785	1.059	0.45	0.183	13.89	− 0.0969
0.08	37.78	1.1	0.371	0.251	13.4	− 0.1622	1.131	0.284	0.333	13.5	− 0.2289
0.1	38.15	1.154	0.408	0.228	13.23	− 0.1453	1.214	0.326	0.303	14.69	− 0.2114
0.15	38.54	1.305	0.511	0.171	13.21	− 0.0993	1.584	0.333	0.302	13.0	− 0.2085
0.2	38.74	1.413	0.637	0.118	14.41	− 0.0653	1.904	0.45	0.22	14.08	− 0.1349
0.3	39.05	1.598	0.79	0.068	14.07	− 0.048	2.418	0.605	0.154	13.87	− 0.1122
0.4	39.31	1.699	0.906	0.035	13.65	− 0.0327	2.598	0.746	0.098	13.67	− 0.0814
0.5	39.52	1.748	0.981	0.016	13.58	− 0.0247	2.597	0.837	0.068	13.54	− 0.0658
0.6	39.47	1.771	1.034	0.004	13.2	− 0.0212	2.537	0.905	0.048	13.3	− 0.057
0.8	39.75	1.77	1.061	− 0.006	12.84	− 0.0139	2.387	0.953	0.029	12.9	− 0.0417
1	39.88	1.753	1.081	− 0.01	12.81	− 0.0127	2.244	0.993	0.017	12.71	− 0.0347
1.5	36.96	1.678	1.14	− 0.028	14.49	0.0033	1.922	1.103	− 0.016	11.32	− 0.0092
2	31.51	1.68	1.116	− 0.019	9.69	− 0.0061	1.841	1.095	− 0.014	10.33	− 0.0103
3	26.91	1.624	1.059	− 0.005	12.06	− 0.0136	1.681	1.037	0.002	12.39	− 0.0181
4	25.34	1.555	1.024	0.005	12.84	− 0.0189	1.567	0.994	0.014	13.78	− 0.0291
5	24.66	1.488	1.004	0.013	13.14	− 0.0253	1.48	0.968	0.023	14.23	− 0.037
6	24.13	1.447	0.975	0.023	13.32	− 0.034	1.404	0.968	0.025	13.95	− 0.0375
8	23.68	1.362	0.963	0.03	13.6	− 0.0402	1.31	0.949	0.034	13.42	− 0.0417
10	23.51	1.303	0.943	0.04	13.83	− 0.0508	1.25	0.937	0.041	14.13	− 0.0495
15	23.42	1.207	0.941	0.049	14.19	− 0.0577	1.156	0.956	0.042	14.57	− 0.0471

The buildup factor is a correction multiplier generated by secondary particles that are essentially related to Compton scattering [62]. Energy Absorption and Exposure Buildup Factors (EABF and EBF) are achieved with Geometric Progression (GP) Fitting Approximation. Equivalent atomic number (Z_{eq}) is determined by matching the $(\mu/\rho)_{Compton}/(\mu/\rho)_{Total}$ ratio of the specific energy with the appropriate ratio of the element. In the recent study, EXABCAL program [63] was employed for buildup factor computations. Tables 5, 6, 7, 8, 9 sum the GP coefficients and Z_{eq} values of BNBD glasses for EABF and EBF

calculations. These tables reveal that the Z_{eq} values of BNBD0 glass has the highest among the others like Z_{eff} . Figures 12 and 13 demonstrate the variation of EABFs and EBFs for BNBD glasses versus the photon energy at several penetration depths. The EABF and EBF get the smallest values in the low and high energy interval for all the glasses. The EABF and EBF values are influenced by the PEA occurring in the low energy zone depending on $Z^{4-5}/E^{3.5}$. Since almost all of the photons are absorbed in this region, photon buildup is very low. However, a small hill is observed on the K- absorption edge of the Ba element

Table 8 Equivalent atomic numbers and G-P Fitting Parameters of EABF and EBF for BNBD15 sample

Energy (MeV)	Zeq	GP- fitting parameters									
		EBF					EABF				
		b	a	c	Xk	d	b	a	c	Xk	d
0.015	18.32	1.01	0.378	0.295	23.61	- 0.3914	1.009	0.408	0.231	24.12	- 0.3333
0.02	23.01	1.014	0.275	0.415	11.16	- 0.3688	1.013	0.31	0.285	14.98	- 0.2401
0.03	23.78	1.038	0.373	0.202	23.29	- 0.2495	1.037	0.333	0.247	16.81	- 0.1759
0.04	35.11	2.486	0.338	0.141	22.63	- 0.0941	1.269	0.37	0.128	27.61	- 0.1744
0.05	35.82	2.161	0.173	- 0.025	14.97	- 0.0329	1.247	0.182	0.053	11.21	0.0002
0.06	36.5	1.057	0.483	0.166	13.99	- 0.0825	1.063	0.443	0.188	13.93	- 0.1007
0.08	37.12	1.106	0.376	0.247	13.44	- 0.1587	1.139	0.292	0.325	13.56	- 0.2219
0.1	37.47	1.163	0.414	0.224	13.27	- 0.1418	1.225	0.34	0.292	15.0	- 0.2033
0.15	37.82	1.319	0.522	0.166	13.27	- 0.0964	1.62	0.342	0.295	13.04	- 0.2037
0.2	37.94	1.433	0.651	0.113	14.35	- 0.0632	1.955	0.466	0.213	14.03	- 0.1319
0.3	38.17	1.619	0.808	0.064	13.95	- 0.0458	2.457	0.629	0.145	13.79	- 0.1074
0.4	38.38	1.716	0.924	0.031	13.48	- 0.0313	2.613	0.771	0.091	13.55	- 0.0776
0.5	38.49	1.761	0.999	0.012	13.27	- 0.0235	2.598	0.864	0.06	13.37	- 0.0618
0.6	38.52	1.78	1.048	0.001	12.83	- 0.0203	2.533	0.927	0.042	13.1	- 0.0537
0.8	38.6	1.778	1.076	- 0.008	12.29	- 0.0137	2.377	0.977	0.023	12.52	- 0.039
1	38.79	1.759	1.092	- 0.012	12.35	- 0.0126	2.234	1.012	0.013	12.23	- 0.0325
1.5	36.27	1.682	1.144	- 0.029	14.79	0.0039	1.924	1.107	- 0.017	11.07	- 0.0091
2	30.59	1.685	1.118	- 0.02	9.41	- 0.0054	1.839	1.101	- 0.016	10.03	- 0.0085
3	26.16	1.626	1.059	- 0.005	12.0	- 0.0133	1.683	1.035	0.002	12.44	- 0.0183
4	24.84	1.557	1.023	0.005	12.78	- 0.0187	1.569	0.993	0.015	13.64	- 0.0288
5	24.14	1.49	1.002	0.013	13.15	- 0.025	1.482	0.967	0.023	14.26	- 0.0365
6	23.79	1.448	0.974	0.023	13.31	- 0.0337	1.406	0.966	0.025	13.88	- 0.0374
8	23.38	1.363	0.961	0.03	13.6	- 0.0399	1.312	0.947	0.034	13.34	- 0.0413
10	23.12	1.304	0.942	0.04	13.8	- 0.05	1.252	0.933	0.041	14.11	- 0.0496
15	23.1	1.208	0.939	0.049	14.16	- 0.0575	1.157	0.956	0.041	14.56	- 0.0463

(37.44 keV) in the composition of the glasses. At middle energies where CS process is effective and secondary scatterings enhance, the EABF and EBF values of BNBD glasses grow and touch a maximum. At high energies (after 1 meV), since the photons are nearly fully annihilated, both buildup factor values reduce all over with the impact of PP. It is noticed from Figs. 12 and 13 that when the concentration of Nb₂O₅ in BNBD glasses enhances from 0 to 20 wt%, the EABF and EBF values decline so that the BNBD0 glass with the largest BaCO₃ concentration takes the

minimum EABF and EBF values. It is also seen from these figures that the photon buildup is less in the glass (EABF) compared to the air (EBF). Figure 14 exhibits the variation of EABF against different penetration depths in 0.15, 1.5, and 15 meV photon energies. At 0.15 meV, EABF tends to increase close to linear with increasing penetration depth. The highest EABF values belong to the BNBD20 glass. The glass chemical composition greatly affects EABF values in that energy. With the prevailing of the CS process at 1.5 meV, the impact of the chemical

Table 9 Equivalent atomic numbers and G-P Fitting Parameters of EABF and EBF for BNBD20 sample

Energy (MeV)	Z_{eq}	GP-fitting parameters									
		EBF					EABF				
		b	a	c	Xk	d	b	a	c	Xk	d
0.015	17.95	1.009	0.49	0.146	28.91	-0.2843	1.009	0.49	0.145	28.93	-0.282
0.02	23.64	1.013	0.243	0.461	11.21	-0.4237	1.013	0.299	0.293	15.7	-0.2523
0.03	24.44	1.035	0.374	0.199	25.13	-0.2701	1.034	0.329	0.248	17.44	-0.1806
0.04	34.42	2.335	0.337	0.152	21.78	-0.0943	1.245	0.372	0.136	27.38	-0.1863
0.05	35.17	2.066	0.189	-0.001	14.79	-0.0423	1.232	0.197	0.07	11.35	-0.012
0.06	35.84	1.061	0.474	0.172	13.95	-0.0867	1.068	0.434	0.193	13.98	-0.1046
0.08	36.41	1.113	0.381	0.243	13.48	-0.1548	1.147	0.3	0.317	13.62	-0.2141
0.1	36.75	1.173	0.421	0.219	13.32	-0.1381	1.237	0.355	0.28	15.33	-0.1945
0.15	37.07	1.334	0.534	0.161	13.32	-0.0933	1.657	0.352	0.289	13.07	-0.1987
0.2	37.16	1.453	0.666	0.108	14.3	-0.0612	2.005	0.482	0.206	13.99	-0.1289
0.3	37.3	1.639	0.826	0.059	13.83	-0.0436	2.496	0.653	0.136	13.7	-0.1026
0.4	37.47	1.732	0.942	0.027	13.31	-0.0297	2.629	0.797	0.083	13.44	-0.0738
0.5	37.48	1.775	1.017	0.008	12.95	-0.0223	2.6	0.892	0.053	13.2	-0.0578
0.6	37.59	1.79	1.063	-0.002	12.46	-0.0193	2.528	0.95	0.036	12.9	-0.0503
0.8	37.83	1.782	1.087	-0.01	11.92	-0.0136	2.369	0.993	0.019	12.26	-0.0372
1.0	37.71	1.764	1.103	-0.014	11.87	-0.0125	2.224	1.032	0.008	11.73	-0.0302
1.5	34.9	1.691	1.151	-0.03	15.41	0.0051	1.929	1.114	-0.019	10.57	-0.009
2.0	30.13	1.688	1.119	-0.02	9.26	-0.0051	1.838	1.105	-0.017	9.88	-0.0076
3.0	25.65	1.628	1.06	-0.005	12.05	-0.0129	1.684	1.036	0.002	12.42	-0.018
4.0	24.35	1.558	1.022	0.005	12.71	-0.0185	1.571	0.992	0.015	13.51	-0.0285
5.0	23.75	1.492	1.0	0.013	13.15	-0.0249	1.484	0.967	0.023	14.29	-0.0361
6.0	23.35	1.449	0.973	0.023	13.3	-0.0334	1.408	0.963	0.025	13.78	-0.0372
8.0	22.98	1.364	0.959	0.03	13.59	-0.0395	1.314	0.946	0.034	13.24	-0.0407
10.0	22.84	1.305	0.942	0.04	13.79	-0.0493	1.254	0.931	0.042	14.09	-0.0498
15.0	22.68	1.209	0.936	0.05	14.13	-0.0572	1.158	0.956	0.04	14.55	-0.0452

composition on EABF curves decrease and EBFs increase linearly with increasing penetration depth for all BNBD glasses. Photon buildup is more for the glasses with large Z_{eq} at high penetration depths at 15 meV prevailed by PP. For this energy, it is seen that the largest EABFs are achieved for the BNBD0 glass.

The ERCS is a measure of the probability of an interaction between fast neutrons and the target. The large ERCS means more the number of interactions per unit time and fast neutron decreasing. ERCS value is found by utilizing equation below [59];

$$ERCS = \sum_i \sum_R (ERCS_e) \quad (11)$$

where ρ denotes the density of i th element and $(ERCS_e)$ refers to the removal cross-section of the i th element. Figure 15 displays the ERCS values of the BNBD glasses. It is obvious that as the Nb_2O_5 concentration rises, the ERCS values of the glasses enhance. This is because the ERCS of Nb replacing Ba is larger than ERCS of Ba element. Also, the increase of Nb_2O_5 addition enhance the glass density. For this reason, it is normal to expect ERCS values to increase.

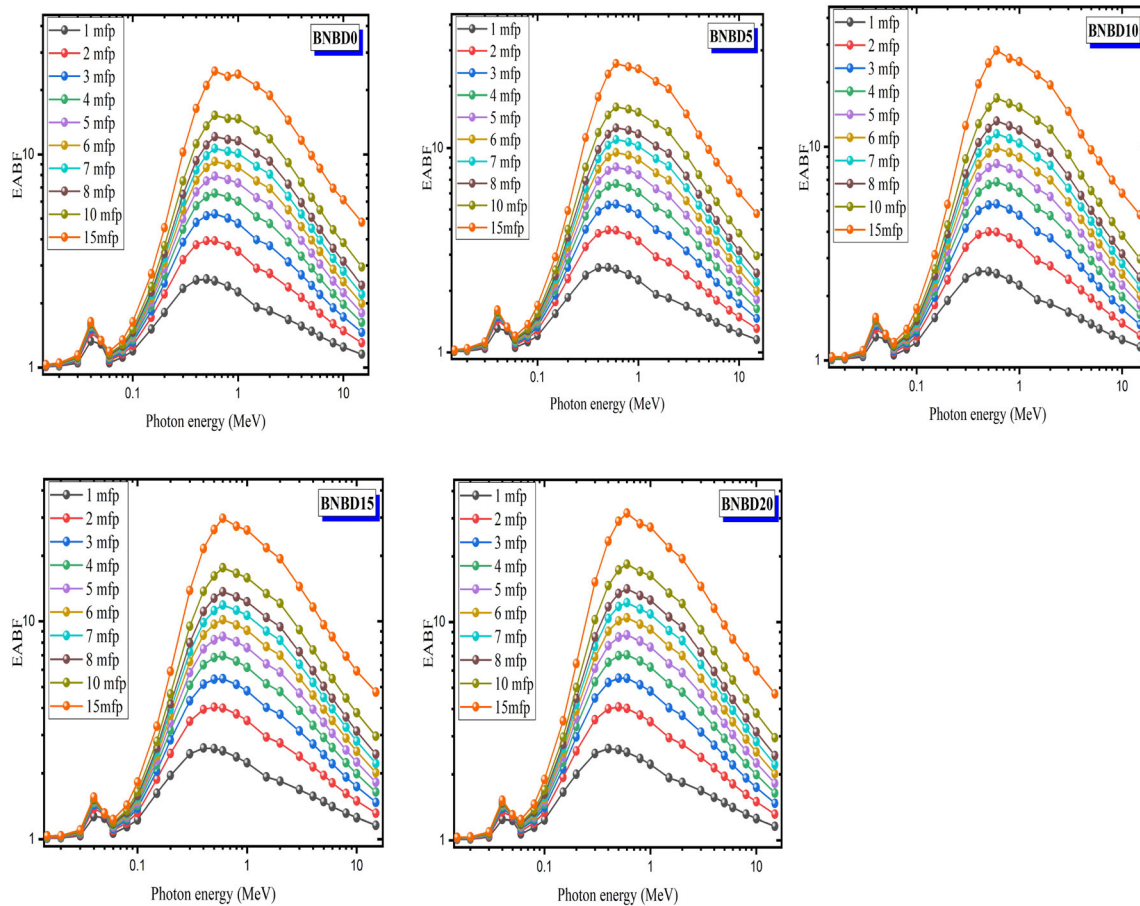


Fig. 12 Variation of energy absorption buildup factor (EABF) with the photon energy for BNBD glasses at different penetration depths (mfp)

From Fig. 15, the ERCS of BNBD glasses change in the range of $0.125\text{--}0.130\text{ cm}^{-1}$. It should be noted that these values are better than the ERCS of water and ordinary concrete (0.101 cm^{-1}), which are preferred as traditional neutron shield.

The passage of high energy electrons from the material is like that of charged particles. Coulomb interaction plays an important role. Scattering occurs because of collisions between relativistic electrons and orbital electrons. Electrons also lose some of their

kinetic energies through Bremsstrahlung radiation. Summing the radiative and electronic (collisional) stopping power of the material is called total stopping power (TSP) [64]. The variation of TSP values of BNBD glasses for electrons is given in Fig. 16 versus the kinetic energy. It is seen that TSP values drop quickly with the increasing kinetic energy of electrons. It was obtained that the TSP values were smaller for the BNBD0 glass. Continuous slowing down approximation (CSDA) range of electrons for

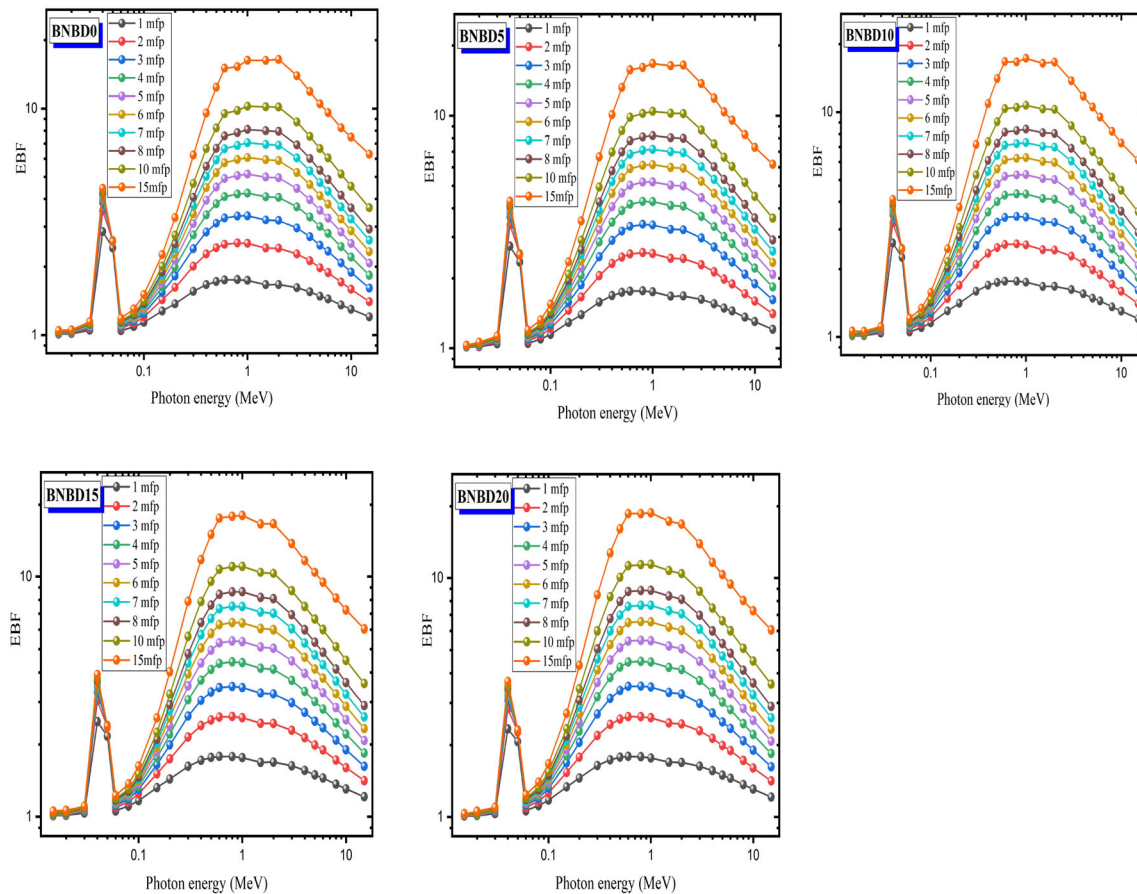


Fig. 13 Variation of exposure buildup factor (EBF) with the photon energy for BNBD glasses at different penetration depths (mfp)

BNBD glass is plotted in Fig. 17 as a function of kinetic energy. Electrons appear to have shorter range in the BNBD0 glass.

4 Conclusion

Five new strontium barium borate glasses doped with dysprosium ion and different concentrations of niobium pentoxide were synthesized using the standard melt-quenching method. The physical, structural, optical, and nuclear-shielding properties of these glasses were investigated. The density and

molar volume values of the prepared glasses were found to increase with increasing niobium content due to the formation of bridging oxygen's. The structural properties like boron-boron distance ($\langle d_{B-B} \rangle$), oxygen packing density (V_o) values increased and the molar volume of oxygen decreased with the niobium content. The number of bonds were found to decrease due to the formation of non-bridging oxygen's.

The oxygen packing density values are found to increase and the molar volume of oxygen decreases with the addition of Nb_2O_5 content which implies that the network is more tightly packed due to the

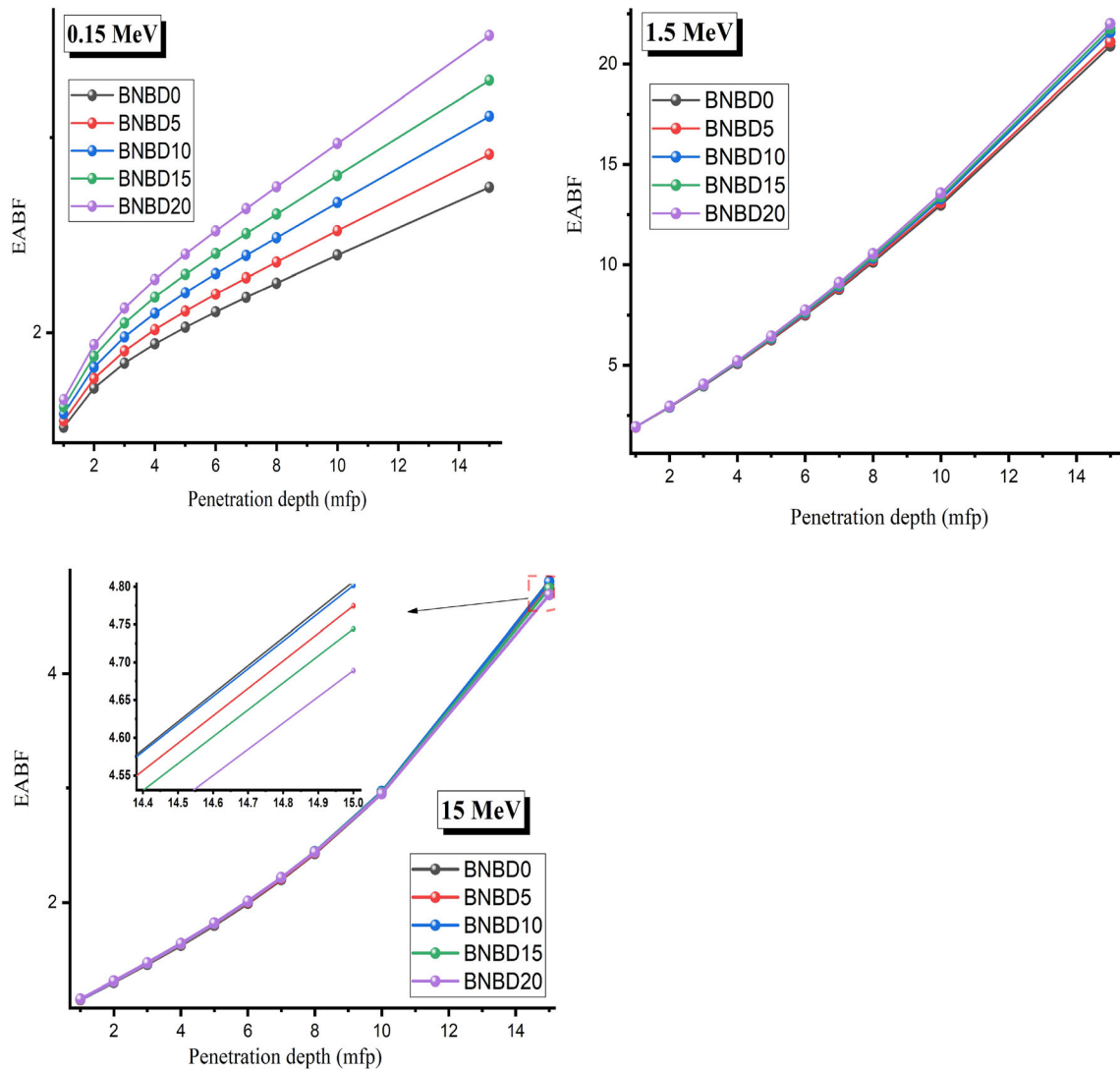


Fig. 14 Variation of energy absorption buildup factor (EABF) with the penetration depth for BNBD glasses at 0.15, 1.5 and 15 meV photon energies

formation of bridging oxygen. The calculated number of bond values are found to decrease from 6.71 to 6.58 while increasing the Nb_2O_5 content. In the present glass network, Poisson’s ratio value is found to be 0.2, thus the system possesses high-cross link density.

The two-photon absorption coefficient (β) values are found to decrease from 13.64 to 10.44 cm/GW . The prepared glass samples in the present system are exceptionally ionic in nature. The direct bandgap values decrease from 3.23 to 2.84 while the indirect

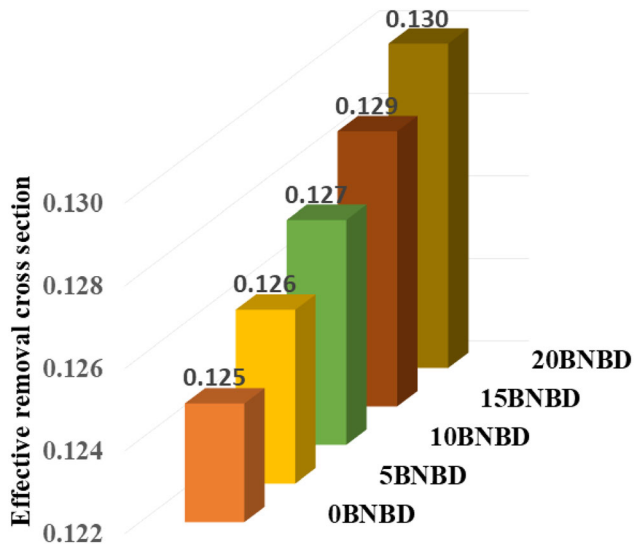


Fig. 15 Effective removal cross sections (Σ_R) of the BNBD glasses

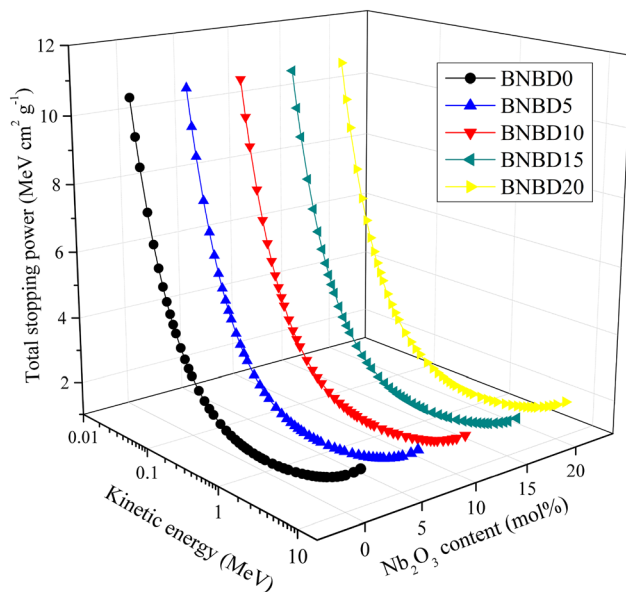


Fig. 16 The variation of total stopping power for electrons versus the electron kinetic energy

bandgap values decrease from 2.8523 to 2.4595 with the increase in Niobium content.

The BNBD0 glass with the highest BaCO₃ content gets the highest μ/ρ values, ranging from 0.033 to 35.430 cm²/g, while the smallest μ/ρ values, varying between 0.0321 and 27.722 cm²/g were obtained for the BNBD20 glass. The prepared glasses possess smaller MFP values than ordinary and barite-added concretes and RS-253-G18 glass, while the MFPs of BNBD glasses are thicker than those of RS-360 and

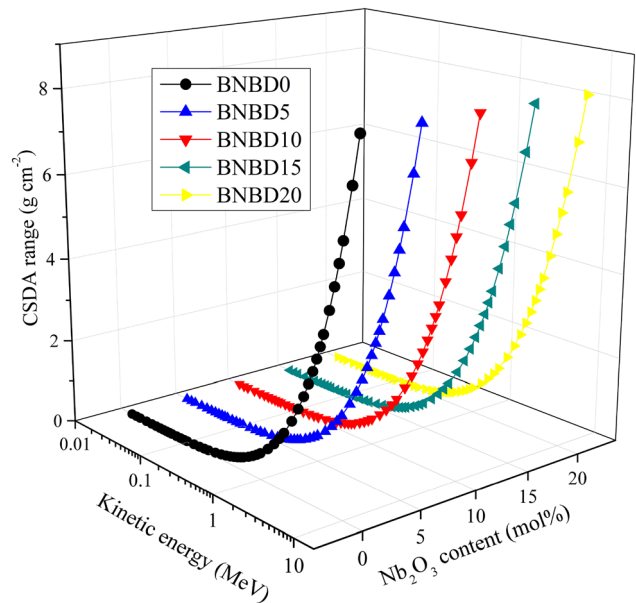


Fig. 17 The variation of CSDA range of electrons for BNBD glasses versus the kinetic energy

AFZT5 glasses. It was concluded that BNBD0 glass with high BaCO₃ concentration can be considered as an alternative material in optical and nuclear radiation shielding applications.

References

1. D.K. Gaikwad, M.I. Sayyed, S.S. Obaid, S.A.M. Issa, P.P. Pawar, J. Alloys Compd. (2018). <https://doi.org/10.1016/j.jallcom.2018.06.240>
2. M. El Okr, M. Farouk, M. El-Sherbiny, M.A.K. El-Fayoumi, M.G. Brik, J. Alloys Compd. (2010). <https://doi.org/10.1016/j.jallcom.2009.07.059>
3. A. Agarwal, A. Sheoran, S. Sanghi, V. Bhatnagar, S.K. Gupta, M. Arora, Spectrochim. Acta Part A Mol. Biomol. Spectrosc. (2010). <https://doi.org/10.1016/j.saa.2009.12.003>
4. M. Abdel-Baki, F.A. Abdel-Wahab, F. El-Diasty, J. Appl. Phys. (2012). <https://doi.org/10.1063/1.3698623>
5. E.A. Abdel Wahab, K.S. Shaaban, R. Elsaman, E.S. Yousef, Appl. Phys. A. (2019). <https://doi.org/https://doi.org/10.1007/s00339-019-3166-8>.
6. W.M. Abd-Allah, H.A. Saudi, K.S. Shaaban, H.A. Farroh, Appl. Phys. A. (2019). <https://doi.org/10.1007/s00339-019-2574-0>
7. M.S. Al-Buriah, F.I. El-Agawany, C. Sriwunkum, H. Akyıldırım, H. Arslan, B.T. Tonguc, R. El-Mallawany, Y.S.

- Rammah, Phys. B Condens. Matter. (2020). <https://doi.org/10.1016/j.physb.2019.411946>
8. K.A. Naseer, P. Karthikeyan, S. Arunkumar, P. Suthanthirakumar, K. Marimuthu, Enhanced luminescence properties of Er³⁺/Yb³⁺ doped zinc tellurofluoroborate glasses for 1.5 μm optical amplification, in: AIP Conf. Proc., 2020: p. 030237. <https://doi.org/10.1063/5.0019171>.
 9. S. ShanmugaSundari, K. Marimuthu, M. Sivraman, S.S. Babu, J. Lumin. (2010). <https://doi.org/10.1016/j.jlumin.2010.02.046>
 10. Q. Chen, K.A. Naseer, K. Marimuthu, P.S. Kumar, B. Miao, K.A. Mahmoud, M.I. Sayyed, J. Aust. Ceram. Soc. (2021). <https://doi.org/10.1007/s41779-020-00531-8>
 11. K.A. Naseer, S. Arunkumar, K. Marimuthu, J. Non. Cryst. Solids. (2019). <https://doi.org/10.1016/j.jnoncrysol.2019.119463>
 12. H.H. Xiong, L.F. Shen, E.Y.B. Pun, H. Lin, J. Lumin. (2014). <https://doi.org/10.1016/j.jlumin.2014.03.029>
 13. E.K. Abdel-Khalek, E.A. Mohamed, A. Ratep, S.M. Salem, I. Kashif, J. Non. Cryst. Solids. (2016). <https://doi.org/10.1016/j.jnoncrysol.2016.03.015>
 14. L. Srinivasa Rao, M. Srinivasa Reddy, M.V. Ramana Reddy, N. Veeraiah, J. Phys. B Condens. Matter. (2008). <https://doi.org/10.1016/j.physb.2008.01.043>
 15. T. Srihari, C.K. Jayasankar, Opt. Mater. (Amst). (2017). <https://doi.org/10.1016/j.optmat.2017.04.001>
 16. N. Krishna Mohan, G. Sahaya Baskaran, N. Veeraiah, J. Phys. Status Solidi. (2006). <https://doi.org/10.1002/pssa.200622093>
 17. A.S. Abouhaswa, M.H.A. Mhareb, A. Alalawi, M.S. Al-Buriahi, J. Non. Cryst. Solids. (2020). <https://doi.org/10.1016/j.jnoncrysol.2020.120130>
 18. I. Boukhris, I. Kebaili, M.S. Al-Buriahi, A. Alalawi, A.S. Abouhaswa, B. Tonguc, Ceram. Int. (2020). <https://doi.org/10.1016/j.ceramint.2020.06.226>
 19. S. Stalin, D.K. Gaikwad, M.S. Al-Buriahi, C. Srinivasu, S.A. Ahmed, H.O. Tekin, S. Rahman, Ceram. Int. (2020). <https://doi.org/10.1016/j.ceramint.2020.10.109>
 20. M.S. Al-Buriahi, V.P. Singh, J. Aust. Ceram. Soc. (2020). <https://doi.org/10.1007/s41779-020-00457-1>
 21. G. Lakshminarayana, A. Kumar, H.O. Tekin, S.A.M. Issa, M.S. Al-Buriahi, D.-E. Lee, J. Yoon, T. Park, J. Mater. Res. Technol. (2020). <https://doi.org/10.1016/j.jmrt.2020.10.019>
 22. K.A. Naseer, K. Marimuthu, M.S. Al-Buriahi, A. Alalawi, H.O. Tekin, Ceram. Int. (2021). <https://doi.org/10.1016/j.ceramint.2020.08.138>
 23. K.A. Naseer, K. Marimuthu, Vacuum (2021). <https://doi.org/10.1016/j.vacuum.2020.109788>
 24. K.A. Naseer, K. Marimuthu, K.A. Mahmoud, M.I. Sayyed, Eur. Phys. J. Plus. (2021). <https://doi.org/10.1140/epjp/s13360-020-01056-6>
 25. M. Dogra, K.J. Singh, K. Kaur, V. Anand, P. Kaur, P. Singh, B.S. Bajwa, Radiat. Phys. Chem. (2018). <https://doi.org/10.1016/j.radphyschem.2017.08.008>
 26. S.H. Elazoumi, H.A.A. Sidek, Y.S. Rammah, R. El-Mallawany, M.K. Halimah, K.A. Matori, M.H.M. Zaid, Results Phys. (2018). <https://doi.org/10.1016/j.rinp.2017.11.010>
 27. S.A.M. Issa, Y.B. Saddeek, H.O. Tekin, M.I. Sayyed, K. SaberShaaban, J. Curr. Appl. Phys. (2018). <https://doi.org/10.1016/j.cap.2018.02.018>
 28. G. Kilic, S.A.M. Issa, E. Ilik, O. Kilicoglu, H.O. Tekin, J. Ceram. Int. (2021). <https://doi.org/10.1016/j.ceramint.2020.09.103>
 29. A. El-Denglawey, H.M.H. Zakaly, K. Alshammari, S.A.M. Issa, H.O. Tekin, W.S. AbuShanab, Y.B. Saddeek, Results Phys. (2021). <https://doi.org/10.1016/j.rinp.2021.103839>
 30. R.M. El-Sharkawy, K.S. Shaaban, R. Elsaman, E.A. Allam, A. El-Taher, M.E. Mahmoud, J. Non. Cryst. Solids. (2020). <https://doi.org/10.1016/j.jnoncrysol.2019.119754>
 31. K.S. Shaaban, H.Y. Zahran, I.S. Yahia, H.I. Elsaedy, E.R. Shaaban, S.A. Makhlof, E.A.A. Wahab, E.S. Yousef, Appl. Phys. A. (2020). <https://doi.org/10.1007/s00339-020-03982-9>
 32. E.A.A. Wahab, K.S. Shaaban, Mater. Res. Express. (2018). <https://doi.org/10.1088/2053-1591/aaee8>
 33. M.S. Al-Buriahi, H. Arslan, H.O. Tekin, V.P. Singh, B.T. Tonguc, Mater. Res. Express. (2020). <https://doi.org/10.1088/2053-1591/ab6db4>
 34. H.A. Saudi, W.M. Abd-Allah, K.S. Shaaban, J. Mater. Sci. Mater. Electron. (2020). <https://doi.org/10.1007/s10854-020-03261-6>
 35. A.F.A. El-Rehim, K.S. Shaaban, H.Y. Zahran, I.S. Yahia, A.M. Ali, M.M.A. Halaka, S.A. Makhlof, E.A.A. Wahab, E.R. Shaaban, J. Inorg. Organomet. Polym. Mater. (2020). <https://doi.org/10.1007/s10904-020-01708-1>
 36. V. Uma, K. Marimuthu, G. Muralidharan, J. Non. Cryst. Solids. (2018). <https://doi.org/10.1016/j.jnoncrysol.2018.03.022>
 37. R. Divina, G. Sathiyapriya, K. Marimuthu, A. Askin, M.I. Sayyed, J. Non. Cryst. Solids. (2020). <https://doi.org/10.1016/j.jnoncrysol.2020.120269>
 38. G. Sathiyapriya, K. Marimuthu, M.I. Sayyed, A. Askin, O. Agar, J. Non. Cryst. Solids. (2019). <https://doi.org/10.1016/j.jnoncrysol.2019.119574>
 39. C.B. Annapurna Devi, S. Mahamuda, M. Venkateswarlu, K. Swapna, A. Srinivasa Rao, G. Vijaya Prakash, J. Opt. Mater. (2016). <https://doi.org/10.1016/j.optmat.2016.11.016>
 40. M.N. Ami Hazlin, M.K. Halimah, F.D. Muhammad, M.F. Faznny, J. Phys. B (2017). <https://doi.org/10.1016/j.physb.2017.01.012>
 41. V. Dimitrov, S. Sakka, J. Appl. Phys. (1996). <https://doi.org/10.1063/1.360963>

42. D.P. Singh, G. Pal Singh, J. Alloys Compd. (2013). <https://doi.org/10.1016/j.jallcom.2012.08.105>
43. M. Çelikbilek Ersundu, A.E. Ersundu, M.I. Sayyed, G. Lakshminarayana, S. Aydin, J. Alloys Compd. (2017). <https://doi.org/10.1016/j.jallcom.2017.04.223>
44. S. Kaur, D. Arora, S. Kumar, G. Singh, S. Mohan, P. Kaur, P. Kriti, P. Kaur, D.P. Singh, J. Lumin. (2018). <https://doi.org/10.1016/j.jlumin.2018.05.034>
45. I.Z. Hager, R. El-Mallawany, J. Mater. Sci. (2010). <https://doi.org/10.1007/s10853-009-4017-3>
46. P. Kaur, K.J. Singh, M. Kurudirek, S. Thakur, Spectrochim Acta Part A (2019). <https://doi.org/10.1016/j.saa.2019.117309>
47. X. Zhao, X. Wang, H. Lin, Z. Wang, Phys. B Condens. Matter. (2008). <https://doi.org/10.1016/j.physb.2008.01.009>
48. K. Swapna, S. Mahamuda, A. Srinivasa Rao, M. Jayasimhadri, T. Sasikala, L. Rama Moorthy, J. Lumin. (2013). <https://doi.org/10.1016/j.jlumin.2013.02.035>
49. N. Vijaya, K. UpendraKumar, C.K. Jayasankar, Spectrochim Acta Part A (2013). <https://doi.org/10.1016/j.saa.2013.04.036>
50. R.J. Amjad, M.R. Sahar, S.K. Ghoshal, M.R. Dousti, R. Arifin, Opt. Mater. (Amst). (2013). <https://doi.org/10.1016/j.optmat.2012.12.024>
51. O. Ravi, C.M. Reddy, B.S. Reddy, B. Deva Prasad Raju, J. Opt. Commun. (2014). <https://doi.org/10.1016/j.optcom.2013.09.044>
52. N. Deopa, A.S. Rao, J. Lumin. (2017). <https://doi.org/10.1016/j.jlumin.2017.07.052>
53. N.F.Mott, E.A. Davis, Electronics Process in Noncrystalline Materials, 1971.
54. M.M. Hivrekar, D.B. Sable, M.B. Solunke, K.M. Jadhav, J. Non. Cryst. Solids. (2018). <https://doi.org/10.1016/j.jnoncrysol.2018.03.051>
55. G. Upender, S. Ramesh, M. Prasad, V.G. Sathe, V.C. Mouli, J. Alloys Compd. (2010). <https://doi.org/10.1016/j.jallcom.2010.06.006>
56. D.S.Z. M.J. Berger, J.H. Hubbel, S.M. Seltzer, J. Chang, J.S. Coursey, R. Sukumar, (2010). <https://doi.org/https://doi.org/10.18434/T48G6X>.
57. M.I. Sayyed, H. Akyildirim, M.S. Al-Buriahi, E. Lacomme, R. Ayad, G. Bonvicini, Appl. Phys. A (2020). <https://doi.org/10.1007/s00339-019-3265-6>
58. SCHOTT, (2018). http://www.schott.com/advanced_optics/english/products/opticalmaterials/special-materials/radiation-shieldingglasses/index.html. Accessed 03 Sept 2018.
59. I.I. Bashter, Ann. Nucl. Energy. (1997). [https://doi.org/10.1016/S0306-4549\(97\)00003-0](https://doi.org/10.1016/S0306-4549(97)00003-0)
60. Y.S. Rammah, A.A. Ali, R. El-Mallawany, F.I. El-Agawany, Phys. B Condens. Matter. (2020). <https://doi.org/10.1016/j.physb.2020.412055>
61. B. Oto, S.E. Gulebaglan, Z. Madak, E. Kavaz, Radiat. Phys. Chem. (2019). <https://doi.org/10.1016/j.radphyschem.2019.03.010>
62. N. Ekinci, E. Kavaz, Y. Özdemir, Appl. Radiat. Isot. (2014). <https://doi.org/10.1016/j.apradiso.2014.05.003>
63. I.O. Olarinoye, R.I. Odiaga, S. Paul, Heliyon. (2019). <https://doi.org/10.1016/j.heliyon.2019.e02017>
64. M.J. Berger, ESTAR, PSTAR and ASTAR: Computer Programs for Calculating Stopping Powers and Ranges for Electrons, Protons and Helium Ions, International Atomic Energy Agency (IAEA), 1995

Publisher's Note Springer Nature remains neutral with regard to jurisdictional claims in published maps and institutional affiliations.